CONFIDENTIAL

NASA TECHNICAL MEMORANDUM

UB
NASA TM X-1475

INVESTIGATION OF HEAT TRANSFER TO LEADING EDGE OF A 76° SWEPT FIN WITH AND WITHOUT CHORDWISE SLOTS AND CORRELATIONS OF SWEPT-LEADING-EDGE TRANSITION DATA FOR MACH 2 TO 8

by Dennis M. Bushnell and Jarrett K. Huffman

Langley Research Center
Langley Station, Hampton, Va.

NATIONAL AERONAUTICS AND SPACE ADMINISTRATION • WASHINGTON, D. C. • DECEMBER 1967

CONFIDENTIAL

NASA TM X-1475

NOFORN

INVESTIGATION OF HEAT TRANSFER TO LEADING EDGE OF A 76° SWEPT FIN WITH AND WITHOUT CHORDWISE SLOTS AND CORRELATIONS OF SWEPT-LEADING-EDGE TRANSITION DATA FOR MACH 2 TO 8

By Dennis M. Bushnell and Jarrett K. Huffman

Langley Research Center
Langley Station, Hampton, Va.

NATIONAL AERONAUTICS AND SPACE ADMINISTRATION

INVESTIGATION OF HEAT TRANSFER TO LEADING EDGE OF A 76° SWEPT FIN WITH AND WITHOUT CHORDWISE SLOTS AND CORRELATIONS OF SWEPT-LEADING-EDGE TRANSITION DATA FOR MACH 2 TO 8*

By Dennis M. Bushnell and Jarrett K. Huffman
Langley Research Center

SUMMARY

Local heat-transfer measurements have been made along the stagnation line of a 76° swept fin mounted on a flat plate. Tests were made with and without both single and multiple chordwise slots cut into the leading-edge region. The tests were conducted at Mach 8 and over a range of free-stream Reynolds numbers based on leading-edge diameter from 2.9×10^4 to 3×10^5. The smooth-fin data are in agreement with laminar and turbulent swept cylinder theory, transition occurring at a Reynolds number of approximately 1.5×10^5. The effect of the slots on the leading-edge heat transfer was to lower the general level of heating below that measured in corresponding tests with the smooth fin.

A review of transition data for smooth swept leading edges at stream Mach numbers from 2 to 8 indicated that transition of the leading-edge boundary layer occurs at free-stream Reynolds numbers, based on leading-edge diameter, from about 1.0×10^5 to 2×10^5 for cylinders having end plates and for fins mounted on flat plates or other adjacent surfaces. However, for delta-wing models and cylinders without end plates or any adjacent surface, leading-edge transition has, in general, not been observed at Reynolds numbers up to 8×10^5 which is the upper limit of the available heat-transfer data for these configurations. The lower transition Reynolds number for the fin-plate configurations indicates that disturbances from the root region propagate along the swept leading edge and cause premature transition of the inherently unstable boundary layer that occurs for these configurations. The data from the large single slot tests indicate that the natural suction associated with the slot partially bled off the stagnation region boundary layer and therefore had the effect of removing these root disturbances. This effect was indicated by the fact that the observed heating level along the leading edge downstream of the slot was in closer agreement with laminar theory for values of free-stream Reynolds numbers (based on diameter) above 2×10^5.

---

*Title, Unclassified.

INTRODUCTION

Current studies of possible configurations for use as hypersonic cruise aircraft generally include the use of highly swept leading edges. These leading edges must be blunted to some degree in order to reduce the local heat transfer. As shown in reference 1, the effect of increasing sweep and leading-edge bluntness is to reduce the local transition Reynolds number. As reference 2 indicates, the leading-edge boundary layer itself may become turbulent; that is, the transition point may be moved forward to the leading edge. In order to be able to predict the heat transfer to a swept leading edge, it is necessary to obtain first a knowledge of the state of the leading-edge boundary layer, that is, a transition criteria must be established.

A previous attempt at correlation of the limited available data in the open literature for "swept cylinders" is presented in reference 3, where a local Reynolds number based on the theoretical laminar spanwise momentum thickness of about 130 seemed to constitute a transition criteria. Subsequent data (ref. 4) indicate that for Mach numbers of 5.3 and 8 and sweep angles of 45° to 68°, a simple transition criterion based on free-stream Reynolds number and leading-edge diameter seems to be successful. However, the lack of high Reynolds number data for large sweep angles (greater than 70°) makes the application of either of these criteria dubious for the large sweep conditions.

The purpose of the present tests is to obtain local-heat-transfer data along the leading edge of a 76° swept fin over a Reynolds number range sufficient to provide for both laminar and turbulent boundary-layer flow. These data, along with some previously unpublished data for a swept cylinder at 72° sweep, are used to determine which of the available leading-edge transition criteria is the most reliable in the high-sweep region. To aid in establishing the best transition criterion, use is made of other available data on swept leading edges. Also, a fin was tested with small chordwise slots to determine the effect of the slots upon local-stagnation-line heat transfer and transition. The slots are intended to simulate typical construction details.

SYMBOLS

c_p	specific heat
D	leading-edge diameter
h	heat-transfer coefficient
k	thermal conductivity

$\dot{m}$	mass flow rate
M	Mach number
η	recovery factor, $\frac{T_{aw} - T_e}{T_o - T_e}$
R	Reynolds number
T	temperature
u	velocity
w	slot width
x	distance along leading edge (fig. 1)
Λ	sweep angle
δ	boundary-layer thickness
μ	viscosity
ρ	density

Subscripts:

aw	adiabatic wall
e	local external to boundary layer
eff	effective
o	stagnation
ref	reference value
slot	slot
w	wall

fp	laminar flat plate
∞	free stream, ahead of leading-edge bow shock (except for referenced flight investigations, where vehicle free stream was used)
D	leading-edge diameter
θ,y	momentum thickness at stagnation line in spanwise direction

APPARATUS

Tunnel

The tests were conducted in the Langley Mach 8 variable-density wind tunnel. This tunnel is of the blowdown type and has an axially symmetric nozzle with contoured walls. The average test-section Mach number variation is from 7.72 to 7.96 for values of stagnation pressure from 100 to 1000 psig (698.5×10^3 to 6985×10^3 N/m^2 gage) (ref. 5). The stagnation temperature varied from 780° F to 1000° F (688° K to 811° K). The test Reynolds number range based on the 0.75-inch (1.905 cm) fin leading-edge diameter and free-stream conditions was from 2.9×10^4 to 3×10^5. The ratio of model wall temperature to tunnel stagnation temperature for the present tests was 0.45 (±0.05).

Models

A sketch of the test configuration is shown in figure 1. Three fins were constructed of high temperature plastic; two were slotted as shown, and the third was identical in outline but without the slots. Photographs of the fins mounted on the plate are shown in figure 2.

The stainless-steel flat plate was 8 inches (0.203 meter) wide and was mounted parallel to the test-section airflow. The fins were swept 76° and the leading-edge diameter was 0.75 inch (0.019 meter). The physical and thermal properties of the plastic used for the fins are as follows:

ρ, lb/ft^3 (kg/m^3)		136 (2180)
c_p, Btu/lb-°R (J/kg-°K)	0.36	(1.5×10^3)
k, Btu/ft-hr-°R (J/m-hr-°K)	0.3	(1.87×10^3)

TEST PROCEDURES AND DATA REDUCTION

Heat-transfer data were obtained on the model by the use of the phase-change-coating technique described in reference 6. This technique, as applied in the present case,

consisted of coating the fin model with a thin layer of a material which undergoes a phase change from solid to liquid at a known temperature. After the initial temperature of the fin was measured, the plate and attached-painted-fin model were injected rapidly into an established airflow, and the time required for the paint to melt at a given station was recorded photographically with a 35-mm camera of known framing rate. (The model was cooled to room temperature between tests.) With the time history of the location of the melt line known from the film record, the local heat-transfer-coefficient distribution was calculated by using the solution of the transient heat conduction equation for a semi-infinite slab with a step input of h (ref. 6). To obtain a value of h from the slab-conduction solution, it is necessary to know T_{aw}. For the present tests a value of recovery factor η of 0.85 was assumed for laminar flow and of 0.89 for turbulent flow. The value of η used in each instance is indicated in the figure when the data are presented. Further details concerning this technique are available in reference 6.

The accuracy of the phase-change-coating technique is discussed in detail in reference 6. Because of the errors discussed in this reference and the probable errors in determining the thermal properties of the model, the final levels of the heat-transfer-coefficient data of the present tests are believed to be accurate to within 25 percent. The maximum scatter is believed to be 10 percent.

DISCUSSION OF TEST RESULTS

Flow Field

Shown in figure 3(a) is a typical schlieren photograph of the weak shock which originates at a plate leading edge. Measurements of shock angle obtained from these photographs at the farthest downstream station visible on the photograph indicated that the flow turning angle would be about 2°. Therefore, the effective sweep of the fin in the present tests was taken as approximately 78°. This measured shock angle was also used to calculate the effective free-stream conditions which would exist in front of the fin bow shock. These "effective" conditions were then used to find values of Reynolds number $R_{\infty,D}$.

Figure 3(b) shows an extrapolation of the leading-edge shock over the portion of the plate occupied by the fin. This figure indicated that the fin was completely inboard of the plate shock and therefore shock-impingement effects were not present for the present fin leading-edge data.

Schlieren photographs of the flow in the vicinity of the fin-plate juncture are shown in figure 4 for both the smooth and multislotted leading-edge models. It is apparent from these photographs that (a) there is no separated flow in the juncture region; (b) the fin bow shock is never exactly parallel to the fin; and (c) as indicated by figure 4(b), the small slots used on the multislotted fin cause no large disturbances to the spanwise flow.

Smooth Fin Model

Shown in figure 5 are three representative distributions of heat-transfer coefficient along the leading edge of the smooth fin. For the low Reynolds number test (fig. 5(a)), the data over most of the fin are in agreement with laminar swept-cylinder theory. There is a region near the root of the fin ($x/D \leqq 3$) where the fin bow shock is forming (see fig. 4(a)) and therefore the local pressure is probably higher and the boundary-layer thickness smaller than would be the case further outboard. These differences could account for the increase in heating in this region. The data shown for an intermediate Reynolds number (fig. 5(b)) tend to approach the laminar theoretical level with increasing x/D, and again, there is an end effect similar to that seen in the previous figure. The high Reynolds number data shown in figure 5(c) are in general agreement with turbulent theory (ref. 2, $T_{ref} = T_e$ as in ref. 4). Figure 5 therefore indicates that the test Reynolds number range was sufficiently large to allow both laminar and turbulent stagnation line flow to be obtained.

In order to obtain the value of transition Reynolds number, data at the $x/D = 12$ station are shown plotted as a function of Reynolds number in figure 6. Also shown are the theoretical variations for laminar and turbulent stagnation line flow. The data indicate that transition at the stagnation line, for the swept fin ($\Lambda_{eff} = 78^{\circ}$) of the present tests, occurred at an $R_{\infty,D}$ value of about 1.5×10^5, which is the same value of transition Reynolds number noted in reference 4 for sweep angles of 45° to 68° and Mach numbers of 5.3 and 7.95. The present tests therefore apparently extend the simple swept-leading-edge transition criterion of reference 4 to a sweep angle of 78°. The question of the further applicability of this criterion is discussed in a subsequent section.

Multislotted Fin Model

Shown in figure 7 is the distribution of heat-transfer coefficient along the stagnation line of the multislotted fin at several different values of Reynolds number. At Reynolds numbers less than or equal to 1×10^5 (figs. 7(a), 7(b), and 7(c)), the heat-transfer data are generally below those predicted by the laminar swept-cylinder theory of reference 2. Also, the data downstream of a given slot exhibit a variation similar to that which occurs in the vicinity of the leading edge of a flat plate. Above a Reynolds number of 1×10^5 (figs. 7(d) to 7(j)), the heat-transfer data immediately downstream of the slots are above those predicted for a laminar stagnation-line boundary layer, and except for the three largest values of $R_{\infty,D}$ (figs. 7(h) to 7(j)) are below the laminar values further downstream. This trend is similar to that exhibited by the data shown in figure 40 of reference 7 (also for multiple slots) where at 10 slot widths downstream the heat-transfer coefficient also fell below laminar theory. (The Reynolds number for the test results shown in figure 40 of reference 7 should be 4.7×10^4 rather than the 4.7×10^6 value given in the figure.) The present trend, however, is different from that of reference 8 where a single

slot was used and the heat transfer decreased monotonically to the laminar value at less than three slot widths downstream of the slot, and then remained at that level. The only pressure data available for a slotted configuration are for the single slot tests of reference 8, where it was found that small increases in pressure occurred immediately downstream of the slot.

To obtain a clearer picture of the variation of the data over the test Reynolds number range, the maximum and minimum values of h measured in the vicinity of the $x/D = 12$ station have been replotted in figure 8. Also shown for reference are the predictions of the theories of reference 2, which were in general agreement with the smooth-fin data (fig. 6). From figure 8 it is evident that the heat transfer increases rapidly with increasing Reynolds number. It is believed that this increase is not due to the occurrence of transition, but rather is a consequence of the increased amount of stagnation-line boundary-layer flow which can be bled off by the slots at the higher Reynolds numbers. The basic flow mechanism whereby a portion of the stagnation-line boundary-layer air is removed or bled off by the slots is due to the difference in pressure between the stagnation-line region and the side of the fin. Therefore, the boundary layer must readjust or partially reform downstream of each slot; that is, each slot creates an end condition similar to that present near the upstream tip of a swept cylinder without an end plate. (See sketch (a).) This "new" boundary layer forms within an existing viscous region which is that portion of the upstream boundary layer not bled off by the slot.

To determine whether the use of this flow model would give results consistent with the trends shown by the data of figure 8, the following discussion is presented. First, the ratio of undisturbed laminar stagnation-line boundary-layer thickness (as calculated by

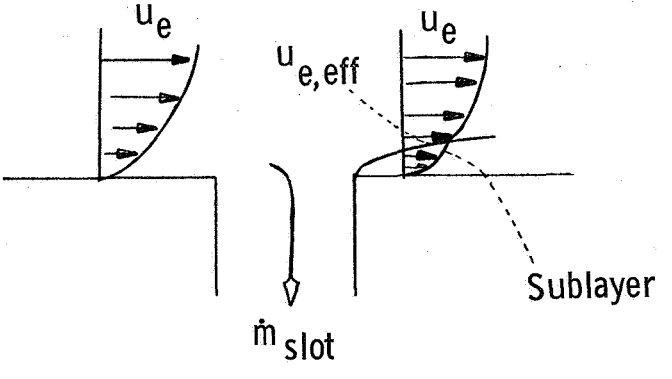

Sketch (a).- Schematic of postulated leading-edge flow in vicinity of a slot

the method of ref. 9) to the slot width is shown in figure 9. From this figure it is evident that for low values of $R_{\infty,D}$, δ and w are about the same order of magnitude. Estimates of the mass flow down the slot indicate values which are roughly 5 percent of the mass flow in the stagnation-region boundary layer for the low Reynolds numbers as compared with 20 percent for the high Reynolds numbers. These estimates of the mass flow in the slot were obtained by solutions of the one-dimensional conservation equations for energy and linear momentum applied to the slot flow. This flow was assumed to expand from the stagnation-line pressure to the pressure level on the side of the fin, the level of which was taken as the free-stream value. Since it was assumed that the inner portion of the viscous flow was bled off, the initial temperature of the slot flow was taken as T_w. Although the slot mass-flow values may be in considerable error because of the approximate nature of the calculations, the calculations do indicate that less than the total mass flow in the stagnation-region boundary layer is bled off by the slots, and that a larger percentage is bled off during the higher Reynolds number tests than at the lower Reynolds numbers.

If the new boundary layer, or sublayer, that forms downstream of each slot is then assumed to be characterized as a flat-plate laminar boundary layer where at a given distance from the slot $h \propto \sqrt{\rho_e u_e \mu_e}$, the ratio of the heat-transfer coefficient h_{eff} with the shear layer present to the value without a shear layer is

$$\frac{h_{eff}}{h_{fp}} \approx \sqrt{\frac{u_{e,eff}}{u_e}}$$

for the assumptions of viscosity proportional to temperature and constant pressure across the shear layer. (Sketch (a) for definition of $u_{e,eff}$.) From the velocity profiles of reference 9, the value of $\frac{u_{e,eff}}{u_e} \approx 0.4$ if 5 percent of the boundary-layer mass flow is removed. The computed values of h_{fp} (figs. 7(a) and 7(b)) behind a typical slot (calculated by the method of ref. 10) would then be reduced by about $\sqrt{0.4} \approx 0.63$. If the concept of a new sublayer downstream of each slot is correct and if conditions external to this sublayer were known with certainty, the data, which were reduced by using T_o to obtain T_{aw}, should be corrected by using the hypothetical-sublayer edge conditions to obtain a value of $T_{aw,eff}$. For the 5-percent bleed case under consideration, $\frac{T_{o,eff}}{T_o} \approx 0.7$ as obtained from the temperature profiles of reference 9 for 5 percent of the boundary-layer mass flow removed. From these quoted effective values of u_e and T_o and with $T_w/T_o = 0.5$, the value of the correction factor $(T_{aw} - T_w)/(T_{aw,eff} - T_w)$ is computed as approximately 2.0 when the recovery factor is taken as 0.85. Therefore, the data would be increased by a factor of about 2 if h were based on the hypothetical edge conditions for the sublayer, and the data would then be in agreement with the theoretical prediction of 0.63 (h_{fp}). At the higher Reynolds numbers where a larger percentage of

the boundary-layer mass flow is removed, the ratio $u_{e,eff}/u_e$ would increase so that the local heat-transfer coefficient would increase and tend to approach the flat-plate level. This expected behavior is apparent in figure 8, where the data appear to be approaching the level corresponding to the indicated h_{fp} range.

The proposed simplified flow model seems to be consistent with both the trends and level of the data shown in figure 8. A similar approach was successfully used in reference 11 for the case of a cone flow expanding onto a cylinder. In this case, the sublayer formed on the cylinder downstream of the expansion from the cone onto the cylinder. However, the sublayer approach for the case of slotted leading edges must be considered as strictly tentative pending further experimental and theoretical investigation.

The present data indicate that for low Reynolds numbers, the stagnation-line heat transfer may be decreased by using small slots; however, as shown in reference 12, a leading-edge slot can cause higher heating along the side of the fin where the high-pressure air exits from the slot. Therefore, the possible reduction in some cases in the leading-edge heating by the use of small slots would probably be offset by the adverse effects which can occur on the wing planform.

Single Slotted Fin Model

Because stagnation-line heat-transfer data for a leading edge with a fairly large single slot is already available for the laminar flow case (ref. 8), in the present tests of the single slotted fin, data were obtained only at high Reynolds numbers, where the leading-edge data on the smooth fin indicated turbulent flow.

The present data for the single slot case are presented in figure 10. The level of the data upstream of the slot ($x/D < 6$) is in general agreement with the results for the smooth fin (see fig. 6) at corresponding Reynolds numbers and indicates turbulent flow upstream of the slot. The increases in heating measured immediately downstream of the slot (in this case the slot is large compared with the boundary-layer thickness) are in agreement with similar trends noted in reference 8.

In the preceding discussion of the multislotted leading-edge data, it was postulated that the level of heating immediately downstream of a slot was a function of the natural suction of the leading-edge viscous flow caused by the slot, and it was noted that a possible explanation of the relative increase in heating in the presence of the slots with Reynolds number (fig. 8) could be the increased suction which would occur as Reynolds number was increased. The single slot data are in agreement since for the same Reynolds numbers, the single slot data (where $w = 0.125$ in.) immediately downstream of the slot are higher than the multislotted data (where $w = 0.030$ in.). For the tests with the larger slot, more natural suction should occur and therefore the heat transfer should increase over that measured for the small slot case.

However, the increase in relative heating with increasing slot size or Reynolds number should occur only when less than 100 percent of the upstream viscous flow is removed by the slot. Once this condition occurs, increases in slot size or Reynolds number (laminar flow being assumed) should no longer cause relative increases in heating, since the external conditions for the viscous flow donwstream of the slot would no longer change appreciably. This result is borne out by the data of reference 8, where for large slots, no appreciable effect of slot width and Reynolds number on relative increases in heating caused by the slot were observed.

It is interesting to note in figure 10 that the level approached by the data downstream of the slot is lower than the turbulent level reached upstream, and that the data are in closer agreement with the theoretical swept cylinder laminar prediction.

In reference 8, where the upstream flow was laminar, the final downstream level was the same as the upstream level. Therefore, the large single slot tested in the present case seems to have the effect of at least partial laminarization of the downstream leading-edge flow. This effect is discussed in the next section which is concerned with the correlation of swept-leading-edge transition data.

SURVEY OF TRANSITION DATA ON SMOOTH SWEPT LEADING EDGES

In order to determine the generality of the simple $R_{\infty,D}$ transition criterion for smooth leading edges and to compare it with the more complex transition criteria based on $R_{\theta,y}$ given in reference 3, a literature survey similar to that of reference 3 was undertaken, except that all available data, including data from classified sources, were used.

The data were divided into two groups. One group involves configurations where there is some adjacent surface with its own flow field or boundary layer that could affect at least the root region of the swept leading edge. Tests of swept cylinders with end plates were assigned to this group as were fin-plate tests. The second group consisted of tests with models having leading edges which were free of any extraneous disturbance, that is, research delta-wing models and fins with sharp or blunted prows. Tests with cylinders attached to plates were assigned to group 1 when the plate was attached to the upstream end of the cylinder, whereas tests with no plates at the upstream end of the cylinder were assigned to group 2. The data were divided into these two different groups because, as indicated in references 13, 14, and 15, disturbances in a root region can propagate along a swept leading edge and affect transition of the entire leading-edge boundary layer.

Two types of correlations are attempted, one using the simple criterion $(R_{\infty,D})$ of reference 4 and the other the slightly more complex criterion $(R_{\theta,y})$ of reference 3.

Included in group 1 data (fin-plate configurations) are the results of tests run on a 72° swept cylinder at $M = 7.95$ during the investigation reported in reference 4 but not presented in that reference. Details of these tests are therefore presented in the appendix of the present paper.

Fin-Plate Type Configurations

Shown in figure 11(a) is the identification of the symbols used in figures 11(b) and 11(c). The data plotted in these figures are for a range of Mach number from 2 to 7.95 and include both wind-tunnel and flight-test data (refs. 16 to 30). The data in terms of the simple $R_{\infty,D}$ parameter are shown plotted in figure 11(b). There are available only a limited number of investigations where transition actually occurred (that is, for most tests the stagnation-line boundary layer was either laminar or turbulent over the entire test range). The transition Reynolds number range is inferred from the state of the stagnation-line boundary layer; laminar, transition, or turbulent by comparison with swept-cylinder heat-transfer theory. Since during the flight tests cited (refs. 21, 23, 25, and 27), the test fins were mounted fairly far back on the carrier vehicle, the assumption was made that the effective "free-stream" Reynolds number for the fins was the same as the free-stream Reynolds number of the carrier vehicle.

From figure 11(b) it is evident that the simple $R_{\infty,D} \approx 2 \times 10^5$ transition criterion is applicable for sweep angles greater than 40°. Within the range of the available data, the effects on transition of Mach number and the ratio of wall temperature to total temperature cannot be discerned. Therefore, for group 1 configurations and sweep angles greater than 40°, the simple transition criterion of reference 4 seems to be of suitable accuracy for engineering use for Mach numbers between 2 and 8.

The transition criterion of reference 3 $\left(R_{\theta,y}\right)$ is of a more general nature than the $R_{\infty,D}$ criterion. The data are plotted in figure 11(c) in terms of the $R_{\theta,y}$ parameter, as calculated by the method of reference 3. From this figure it is evident that a value of $R_{\theta,y}$ of around 200 would seem to be a reasonable transition criterion over the entire sweep angle range. The fact that the data correlate in terms of $R_{\theta,y}$ as well as $R_{\infty,D}$ for $\Lambda > 40^{\circ}$ indicates that $R_{\theta,y}$ is not a strong function of Mach number and sweep angle for sweep angles greater than 40°, since $R_{\theta,y} = f\left(R_{\infty,D}, M_{\infty}, \Lambda\right)$. For extrapolation up to higher Mach numbers, the $R_{\theta,y}$ criterion would presumably be superior because it includes an effect of Mach number. However, because of its simplicity, for the range of applicability noted previously, the $R_{\infty,D}$ criterion would probably be more convenient to use.

Undisturbed-Leading-Edge Configurations

The data for the second group of configurations are shown in figure 12. Again, part (a) is an identification of the various symbols used in parts (b) and (c). The Mach number range of the data is from 2.5 to 10. The data are plotted in figure 12(b) in terms of the $R_{\infty,D}$ parameter. It is apparent from the figure that only in one investigation has turbulent flow been obtained along the leading edge. As shown, the data available (refs. 31 to 45) indicate that the transition Reynolds number for these types of models is of the order of 8×10^5 or greater, a value which is a factor of 4 above the value for the fin-plate configurations already discussed. As only one investigation has obtained turbulent leading-edge flow for these types of configurations, it is not yet clear when transition would occur on these shapes, especially on those with sharp prows. For shapes with blunt prows at high enough $R_{\infty,D}$, transition due to conventional instabilities could occur in the nose region before the flow reaches the leading edge. Presumably, this condition could cause turbulent flow to occur along the leading edge, whereas with a sharp prow the flow might be laminar. This condition may be the cause of the transition for the turbulent data shown in figure 11(b) since the model used was very blunt (ref. 44). Therefore, as one would expect from the discussion of references 13, 14, and 15, leading-edge transition is delayed where there is no root disturbance.

The data are plotted in terms of the $R_{\theta,y}$ parameter in figure 12(c), and when this figure is compared with figure 11(c), conclusions similar to those for figure 12(b) can be drawn; that is, the transition Reynolds number for these "undisturbed" configurations is considerably higher than that for the fin-plate type of models.

As an adjunct to this conclusion, it is pointed out that as reported in reference 16, tests were conducted with a 45^o swept right circular cylinder attached to a plate and swept forward and rearward. For the tests with the cylinder swept forward (there was no end plate and the end of the cylinder was parallel to the airstream), there would be a minimum of root disturbance. The heating rate for this case was consistently at most a third of that measured on the cylinder when it was swept rearward. For the rearward sweep case, the contamination from the plate boundary-layer flow could propagate along the leading-edge boundary layer on the cylinder. These tests support the general conclusion arrived at by comparison of figures 11(b) and 12(b) or 11(c) and 12(c) that the root contamination causes early transition of the leading-edge boundary layer.

In connection with the conclusion that leading-edge transition is caused by "root" contamination, there is a possibility that one or more large slots similar to those used in the present case, if located on the fin near a juncture region, could be used to bleed off "disturbed" leading-edge flow and thereby delay transition. A similar concept, using a "bump," was proposed in reference 13. As reported in references 14 and 15, both slots and bumps have been used successfully at subsonic speeds in connection with the X-21

program. The present results for the single slot tests (fig. 10) indicate that the effect of a large slot is to bleed off the "disturbed" root flow. As noted in the discussion of the present single slot data, the data downstream of the slot are in closer agreement with the laminar prediction than the turbulent prediction, whereas the level upstream of the slot was in agreement with the turbulent prediction. This result indicates that partial laminarization of the leading-edge flow occurred because of the action of the slot. Much more work will have to be done toward optimization of a slot configuration, especially the decreasing of the interference heating on the sides of the fin (ref. 12). Also, it may be possible to modify the downstream lip of the slot and decrease the high heating immediately downstream, without compromising the ability of the slot to make the flow laminar.

CONCLUSIONS

An investigation has been conducted of the heat transfer to a 76° swept fin with and without single and multiple chordwise slots and mounted on a plate. The tests were conducted at Mach 8 and over a Reynolds number range of 2.9×10^4 to 3×10^5 based on effective free-stream conditions ahead of the fin bow shock and fin leading-edge diameter. The following conclusions can be made:

1. The heat transfer along the smooth-fin stagnation line could be predicted by swept cylinder theory for both the laminar and turbulent boundary-layer conditions.

2. Transition of the leading-edge boundary layer for the smooth fin occurred at a value of free-stream Reynolds number, based on leading-edge diameter, of approximately 1.5×10^5.

3. The effect of the chordwise slots at low Reynolds numbers is to lower the general level of heating along the leading edge below the corresponding plain fin value. A plausible flow model is proposed that appears to be consistent with the trends and level of the observed heating. The data for the single slot indicate that partial laminarization of the leading-edge flow occurred and was evidently caused by the slot.

4. A survey of heat-transfer data on swept leading edges indicates that root contamination from the region of intersection with an adjoining body causes transition to occur at a much lower Reynolds number than for an "undisturbed" leading edge such as a delta-wing model.

5. A simple transition criterion of a Reynolds number based on free-stream conditions and leading-edge diameter of 2×10^5 is generally applicable for sweep angles greater than 40° and for Mach numbers from 2 to 8 for the case where root contamination of the leading-edge flow occurs. For configurations having "undisturbed" leading-edge flow, the transition Reynolds number is in excess of 8×10^5, and the actual value is not

presently known because of a scarcity of data for undisturbed configurations above Reynolds numbers of 8×10^5.

6. For the "disturbed" leading-edge flows, a transition criterion of Reynolds number based on local conditions and spanwise momentum thickness $R_{\theta,y}$ of approximately 200 is generally applicable for sweep angles greater than 10^o and for Mach numbers from 2 to 8.

Langley Research Center,
National Aeronautics and Space Administration,
Langley Station, Hampton, Va., August 3, 1967,
129-01-08-38-23.

APPENDIX

HEAT-TRANSFER DATA OBTAINED ALONG THE STAGNATION LINE OF A 72° SWEPT RIGHT CIRCULAR CYLINDER

The purpose of this appendix is to present the results of an investigation of the local heat transfer along the stagnation line of a right circular cylinder swept 72° with respect to the free-stream flow. The data were obtained during the investigation reported in reference 4 but have not been previously published. Details as to model construction, instrumentation, and test procedures, and data reduction are available in that reference. However, a brief summary of this information is given here.

The data were obtained by the transient heating technique using a thin-skinned thermocouple-instrumented model. The tests were conducted in the Mach 8 variable-density tunnel, the same facility as was used in the present swept fin tests.

The only difference between the model used in reference 4 and the one used to obtain the 72° swept cylinder data reported herein is that the size of the elliptically shaped end plate used to cap the cylinder was reduced so that instead of a protrusion of 0.25 inch (0.635 cm) from the outside of the cylinder, the protrusion was 0.12 inch (0.305 cm). This modification was made in an attempt to reduce tip interference on the cylinder stagnation-line flow. In the present tests both the end of the cylinder and the top of the end plate were parallel to the free-stream flow.

Schlieren photographs of the flow over the cylinder in the vicinity of the end plate are shown in figure 13 for two values of Reynolds number. From these photographs it is evident that the cylinder bow shock does not become parallel to the cylinder for several diameters from the tip. Also apparent is that the end plate seems to cause only a small disturbance to the cylinder bow shock, as would be expected because of the small size of the end plate and the fact that it is parallel to the free-stream flow. Schlieren photographs shown in reference 4 indicate a much larger disturbance caused by the end plate used therein.

The stagnation-line heat-transfer distribution is shown in figure 13 where the measured heat-transfer coefficient has been plotted against the distance along the stagnation line from the end of the cylinder where the end plate is attached. The data of figure 14(a) are for a low Reynolds number test, and the data are in agreement with laminar swept cylinder theory (ref. 2) where a bow shock swept parallel to the cylinder has been assumed. The distribution along the cylinder is fairly flat; thus, the flow at least approximates that over an infinite swept cylinder. The data for an intermediate Reynolds number are shown in figure 14(b). The data, although a fairly flat distribution is indicated, have a level which is between the laminar and turbulent swept cylinder theories (the

turbulent theory is again from reference 2 where T_{ref} has been assumed equal to T_e as in ref. 4). The high Reynolds number data are shown in figure 14(c). The data at small x/D values (near the tip or end plate) begin at a transitional level but become fully turbulent for $x/D > 4$. Evidently, the stagnation-line boundary layer requires a finite spanwise distance to become completely turbulent, at least for the high sweep angle of these tests. Data for a 60^o swept cylinder shown in reference 4 indicate a similar phenomenon.

A summary plot of the measured heat-transfer coefficient as a function of Reynolds number at $x/D = 4.3$ is shown in figure 15. Also shown in this plot are the turbulent and laminar swept cylinder theories. Comparison of the measured data with the theories indicates that although transition begins to occur at $R_{\infty,D} \approx 1.5 \times 10^5$ and is in agreement with the data of reference 4 for $45^o \leqq \Lambda \leqq 68^o$, the smaller end plate appears to delay the development of fully turbulent stagnation-line flow until a higher Reynolds number; that is, the flow appears to be transitional over a wider range of Reynolds number.

REFERENCES

1. Jillie, Don W.; and Hopkins, Edward J.: Effects of Mach Number, Leading-Edge Bluntness, and Sweep on Boundary-Layer Transition on a Flat Plate. NASA TN D-1071, 1961.

2. Beckwith, Ivan E.; and Gallagher, James J.: Local Heat Transfer and Recovery Temperatures on a Yawed Cylinder at a Mach Number of 4.15 and High Reynolds Numbers. NASA TR R-104, 1961. (Supersedes NASA MEMO 2-27-59L.)

3. Topham, D. R.: A Correlation of Leading Edge Transition and Heat Transfer on Swept Cylinders in Supersonic Flow. J. Roy. Aeronaut. Soc., vol. 69, no. 649, Jan. 1965, pp. 49-52.

4. Bushnell, Dennis M.: Interference Heating on a Swept Cylinder in Region of Intersection With a Wedge at Mach Number 8. NASA TN D-3094, 1965.

5. Stainback, P. Calvin: Heat-Transfer Measurements at a Mach Number of 8 in the Vicinity of a 90^{o} Interior Corner Alined With the Free-Stream Velocity. NASA TN D-2417, 1964.

6. Jones, Robert A.; and Hunt, James L.: Use of Fusible Temperature Indicators for Obtaining Quantitative Aerodynamic Heat-Transfer Data. NASA TR R-230, 1966.

7. Jaeck, C. L.: Analysis of Pressure and Heat Transfer Tests on Surface Roughness Elements With Laminar and Turbulent Boundary Layers. NASA CR-537, 1966.

8. Burchfield, C. G.; and Bontrager, P. J.: Pressure and Heat-Transfer Measurements on a Slotted Leading Edge in Hypersonic Flow. AEDC-TR-66-100, U.S. Air Force, May 1966. (Available from DDC as AD 481634.)

9. Reshotko, Eli; and Beckwith, Ivan E.: Compressible Laminar Boundary Layer Over a Yawed Infinite Cylinder With Heat Transfer and Arbitrary Prandtl Number. NACA Rept. 1379, 1958. (Supersedes NACA TN 3986.)

10. Beckwith, Ivan E.; and Cohen, Nathaniel B.: Application of Similar Solutions to Calculation of Laminar Heat Transfer on Bodies With Yaw and Large Pressure Gradient in High-Speed Flow. NASA TN D-625, 1961.

11. Zakkay, Victor; Toba, Kaoru; and Kuo, Ta-Jin: Laminar, Transitional, and Turbulent Heat Transfer After a Sharp Convex Corner. AIAA J., vol. 2, no. 8, Aug. 1964, pp. 1389-1395.

12. Kordes, Eldon E.; Reed, Robert D.; and Dawdy, Alpha L.: Structural Heating Experiences on the X-15 Airplane. NASA TM X-711, 1962.

13. Gaster, M.: On the Flow Along Swept Leading Edges. $C_{O}A$-AERO-167, College of Aeron. (Engl.), Oct. 1965.

14. Braslow, Albert L.: A Review of Factors Affecting Boundary-Layer Transition. NASA TN D-3384, 1966.

15. Pfenninger, Werner; and Reed, Verlin D.: Laminar-Flow Research and Experiment. Astronaut. Aeronaut., vol. 4, no. 7, July 1966, pp. 44-50.

16. Jones, Robert A.; and Trimpi, Robert L.: Heat-Transfer and Pressure Distributions at a Mach Number of 6 for 70° Swept Slab Wings With Sharp and Spherical Noses and Cylindrical Leading Edges. NASA TM X-682, 1962.

17. Beckwith, Ivan E.; and Gallagher, James J.: Experimental Investigation of the Effect of Boundary-Layer Transition on the Average Heat Transfer to a Yawed Cylinder in Supersonic Flow. NACA RM L56E09, 1956.

18. Burbank, Paige B.; Newlander, Robert A.; and Collins, Ida K.: Heat-Transfer and Pressure Measurements on a Flat-Plate Surface and Heat-Transfer Measurements on Attached Protuberances in a Supersonic Turbulent Boundary Layer at Mach Numbers of 2.65, 3.51, and 4.44. NASA TN D-1372, 1962.

19. Price, Earl A.; Howard, Paul W.; and Stallings, Robert L., Jr.: Heat-Transfer Measurements on a Flat Plate and Attached Fins at Mach Numbers of 3.51 and 4.44. NASA TN D-2340, 1964.

20. Jones, Robert A.: Heat-Transfer and Pressure Investigation of a Fin-Plate Interference Model at a Mach Number of 6. NASA TN D-2028, 1964.

21. Howard, Floyd G.: Heat Transfer on Unswept and 38° Swept Cylindrically Blunted Wedge Fins in Free Flight to Mach Number 4.11. NASA TN D-2386, 1964.

22. Bushnell, Dennis M.; and Jones, Robert A.: Heat Transfer to a 70° Swept Fin Partly Submerged in a Turbulent Boundary Layer at Mach 6. NASA TM X-1191, 1965.

23. O'Neal, Robert L.: Heat Transfer to 36.75° and 45° Swept Blunt Leading Edges in Free Flight at Mach Numbers From 1.70 to 2.99 and From 2.50 to 4.05. NASA TM X-208, 1960.

24. Hiers, R. S.: Heat Transfer to Protuberances Partially Immersed in a Hypersonic, Turbulent Boundary Layer. AEDC TDR-62-66, U.S. Air Force, Apr. 1962.

25. O'Neal, Robert L.; and Bond, Aleck C.: Heat Transfer to 0° and 75° Swept Blunt Leading Edges in Free Flight at Mach Numbers From 1.90 to 3.07. NASA TN D-1256, 1962.

26. Goodwin, Glen; Creager, Marcus O.; and Winkler, Ernest L.: Investigation of Local Heat-Transfer and Pressure Drag Characteristics of a Yawed Circular Cylinder at Supersonic Speeds. NACA RM A55H31, 1956.

27. Speegle, Katherine C.: Heat-Transfer Measurements of Two Wing-Body Combinations at 8^{o} Angle of Attack From a Flight Test for Mach Numbers to 4.86 and Reynolds Numbers to 19.2×10^{6}. NASA MEMO 10-25-58L, 1958.

28. Anon.: Analysis of Wind Tunnel Tests at Mach 6 To Determine Heat Transfer Coefficients. Doc. No. D5-4382, Boeing Airplane Co., 1959.

29. Diep, Gia Ban; Le Fur, Bernard; and Brun, E. A.: Heat and Mass Transfer on Sweptback Circular Cylinders in Supersonic Flow. Proceedings of the Third International Heat Transfer Conference, vol. II, Am. Inst. Chem. Eng., Aug. 1966.

30. Thomann, H. (W.J.G. Pinsker, Trans.): Measurements of Heat Transfer Coefficient, Temperature and Pressure Distribution on a Delta Wing at $M = 3.0$. Libr. Trans. No. 964, British R.A.E., Sept. 1961.

31. Feller, William V.: Investigation of Equilibrium Temperatures and Average Laminar Heat-Transfer Coefficients for the Front Half of Swept Circular Cylinders at a Mach Number of 6.9. NACA RM L55F08a, 1955.

32. Bertram, Mitchel H.; and Everhart, Philip E.: An Experimental Study of the Pressure and Heat-Transfer Distribution on a 70^{o} Swept Slab Delta Wing in Hypersonic Flow. NASA TR R-153, 1963.

33. Stainback, P. Calvin: Heat-Transfer Measurements at a Mach Number of 4.95 on Two 60^{o} Swept Delta Wings with Blunt Leading Edges and Dihedral Angles of 0^{o} and 45^{o}. NASA TN D-549, 1961.

34. Whitehead, Allen H., Jr.; and Dunavant, James C.: A Study of Pressure and Heat Transfer Over an 80^{o} Sweep Slab Delta Wing in Hypersonic Flow. NASA TN D-2708, 1965.

35. Nagel, A. L.; Fitzsimmons, H. D.; and Doyle, L. B.: Analysis of Hypersonic Pressure and Heat Transfer Tests on Delta Wings With Laminar and Turbulent Boundary Layers. NASA CR-535, 1966.

36. Stallings, Robert L., Jr.; Burbank, Paige B.; and Howell, Dorothy T.: Heat-Transfer and Pressure Measurements on Delta Wings at Mach Numbers of 3.51 and 4.65 and Angles of Attack From -45^{o} to 45^{o}. NASA TN D-2387, 1964.

37. Gunn, Charles R.: Heat-Transfer Measurements on the Apexes of Two 60^{o} Sweptback Delta Wings (Panel Semiapex Angle of 30^{o}) Having 0^{o} and 45^{o} Dihedral at a Mach Number of 4.95. NASA TN D-550, 1961.

38. Everhart, Philip E.; and Dunavant, James C.: Heat-Transfer Distribution on 70^{o} Swept Slab Delta Wings at a Mach Number of 9.86 and Angles of Attack up to 90^{o}. NASA TN D-2302, 1964.

39. Dunavant, James C.: Investigation of Heat Transfer and Pressures on Highly Swept Flat and Dihedraled Delta Wings at Mach Numbers of 6.8 and 9.6 and Angles of Attack to 90°. NASA TM X-688, 1962.

40. Royall, John F., Jr.; and Newcomb, John F.: Investigation of Heat Transfer on a Simulated 82° Swept Delta Wing in Free Flight at Angle of Attack at Mach Numbers up to 9.8. NASA TM X-622, 1962.

41. Samet, S.; and Isenberg, J. S.: An Experimental Investigation of Hypersonic Aerodynamic Heating on Highly Swept Delta Wing Configurations. ASD-TDR-62-798, U.S. Air Force, Mar. 1963.

42. Hiers, R. S.; and Hillsamer, M. E.: Heat Transfer and Pressure Distribution Tests on Three Blunted Delta Wing Shapes. AEDC-TN-60-225, U.S. Air Force, Dec. 1960.

43. Hiers, R. S.; and Hillsamer, M. E.: Heat Transfer and Pressure Distribution Tests of the Leading Edge Region of a Nike-Zeus Canard at Mach 4, 6, and 8. AEDC-TN-61-135, U.S. Air Force, Oct. 1961.

44. Hillsamer, M. E.; Hube, F. K.; and Palko, R. L.: Heat Transfer and Pressure Distribution Tests of the Leading Edge Region of a Nike-Zeus Canard at Mach 4, 6, and 8. AEDC-TDR-62-179, U.S. Air Force, Oct. 1962.

45. Anon.: Analysis of Wind Tunnel Heat Transfer Tests at M = 6. Doc. No. D5-4381, Boeing Aircraft Co., 1959.

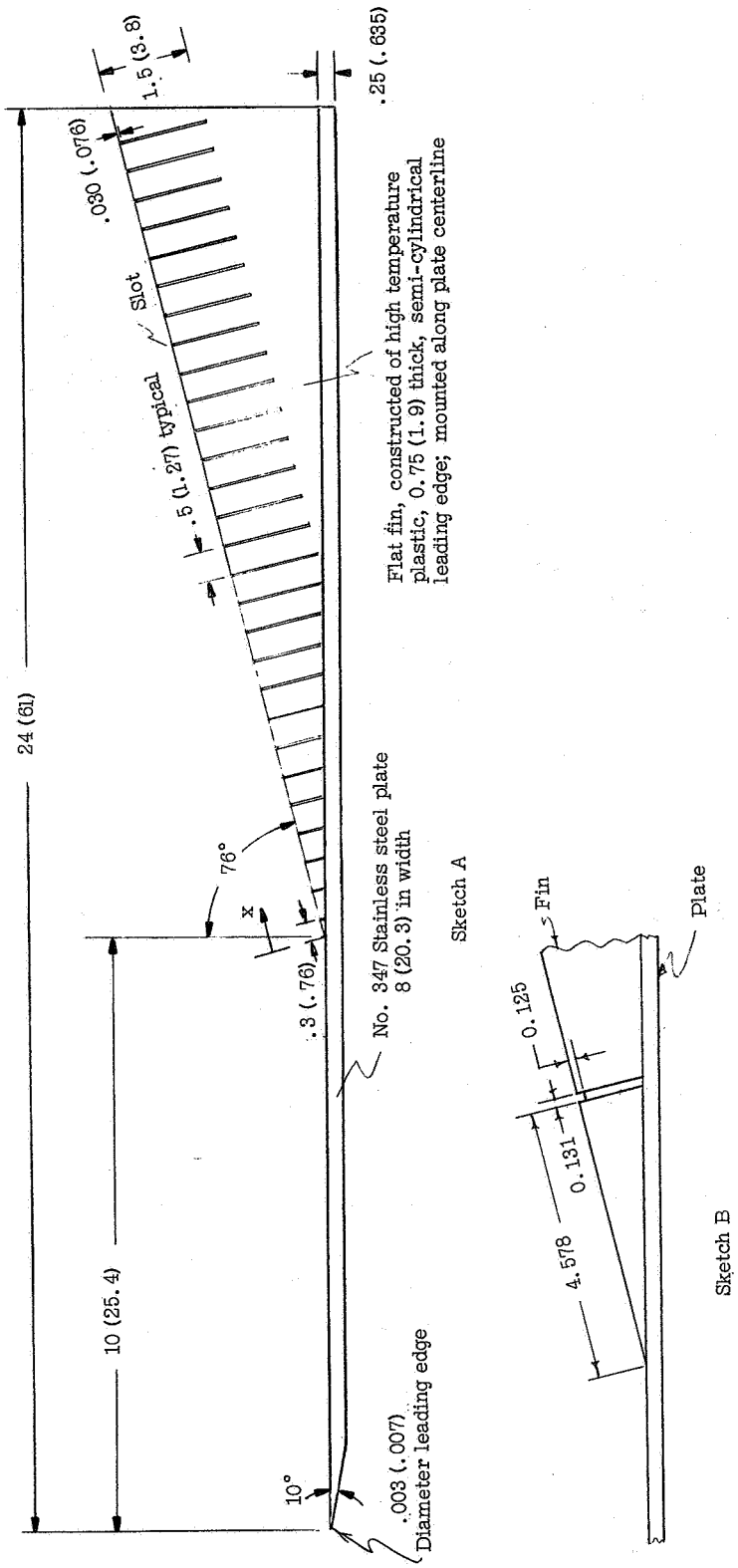

Figure 1.- Sketches of models. Linear dimensions are in inches; values in parentheses are in centimeters.

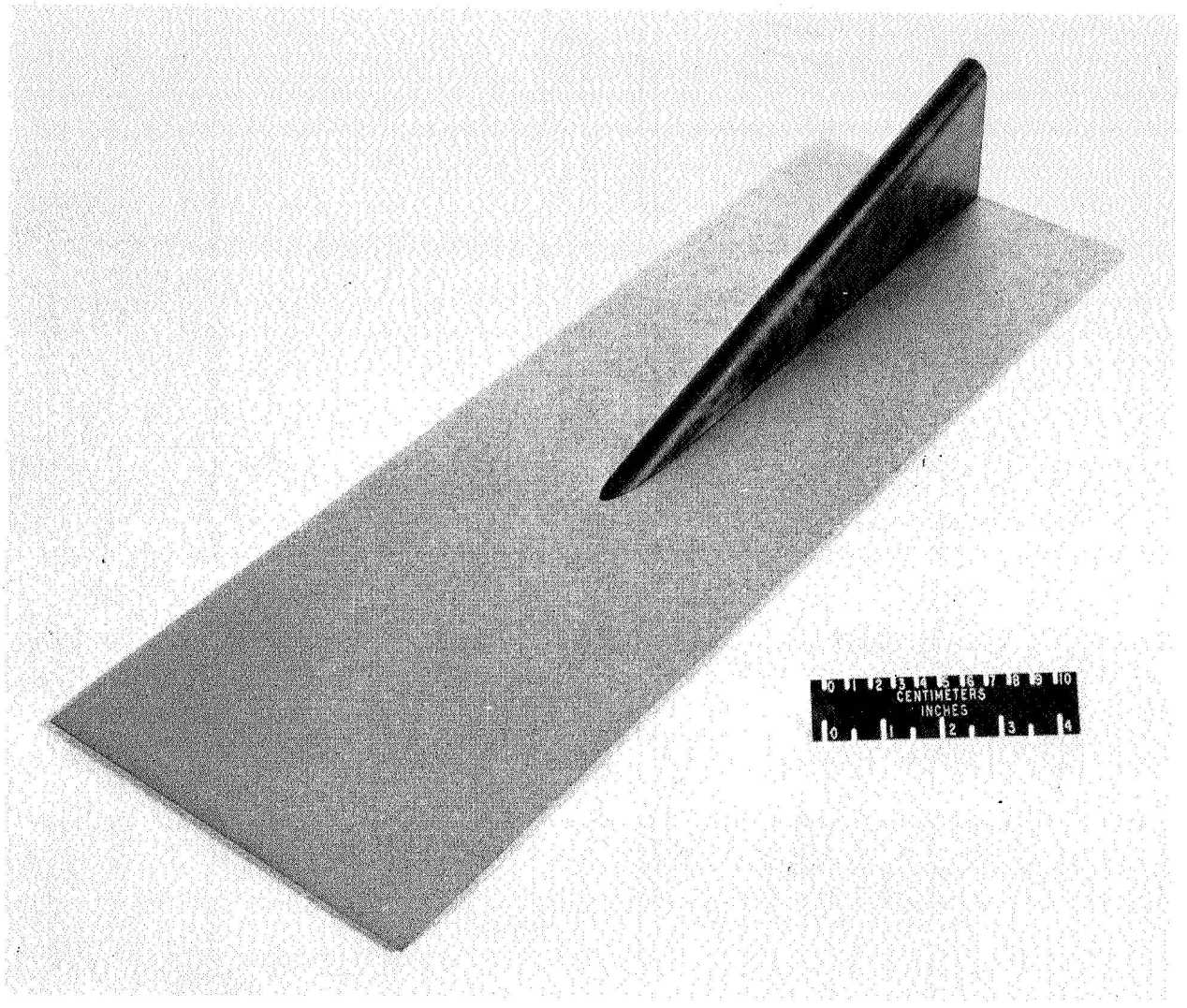

(a) Smooth leading-edge model. L-66-9170

Figure 2.- Photographs of fin models mounted on plate.

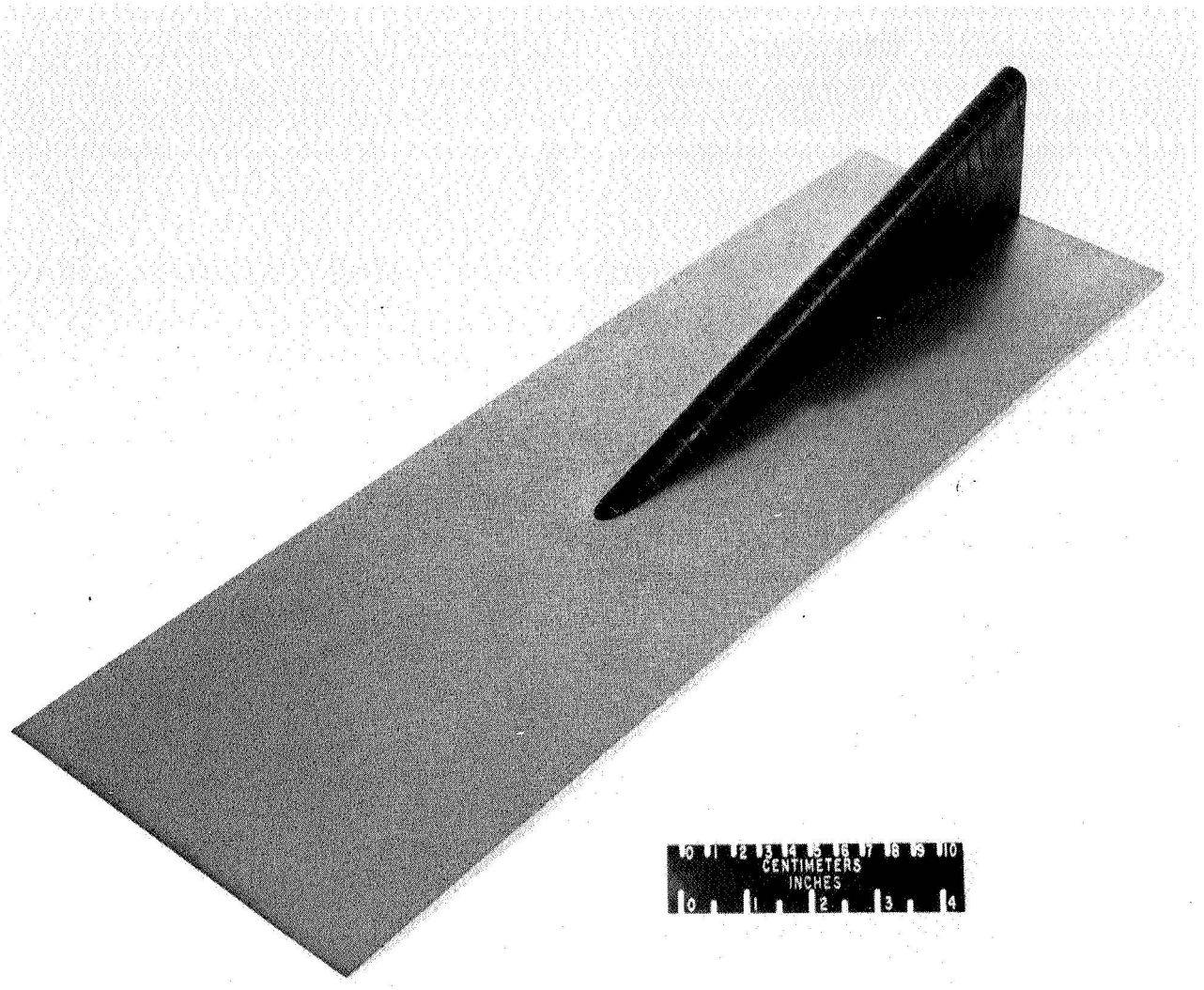

(b) Multislotted leading-edge model. L-66-9171

Figure 2.- Continued.

L-67-5098

(c) Single slotted leading-edge model.

Figure 2.- Concluded.

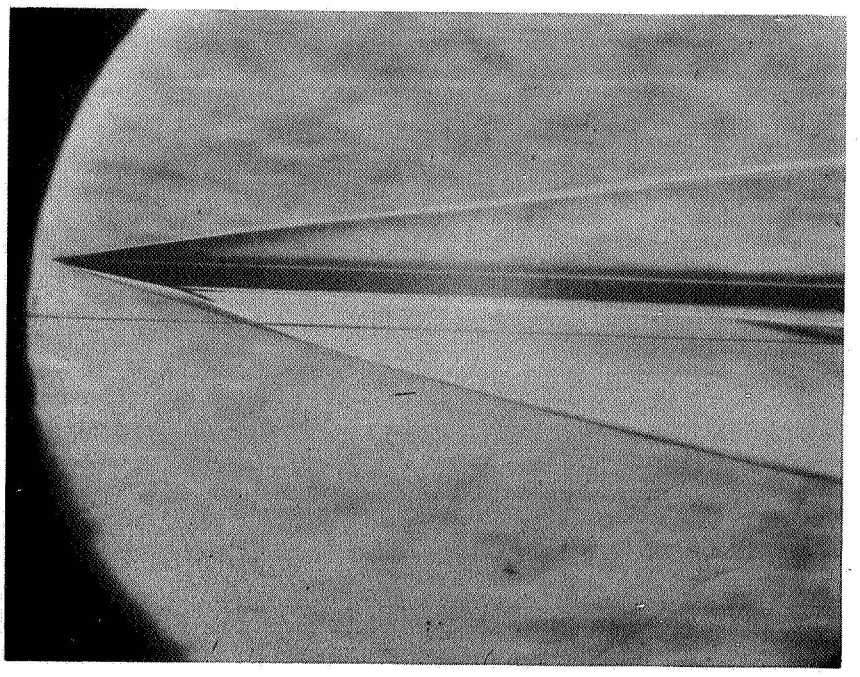

L-67-6629

(a) Schlieren photograph showing leading edge of flat plate and weak plate leading-edge shock.

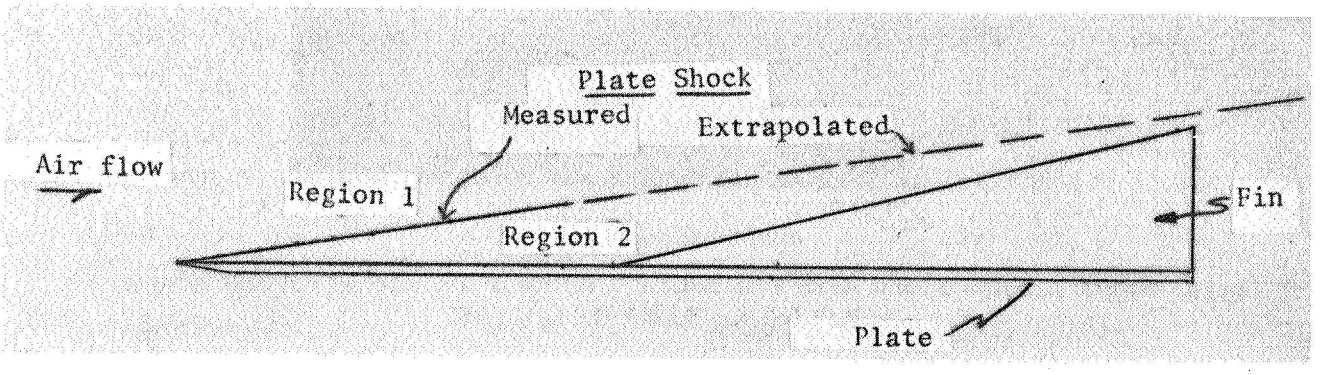

(b) Sketch showing that extrapolated plate shock would not intersect model.

Figure 3.- Schlieren photograph and sketch of flow field showing position of plate leading-edge shock in relation to fin leading edge.

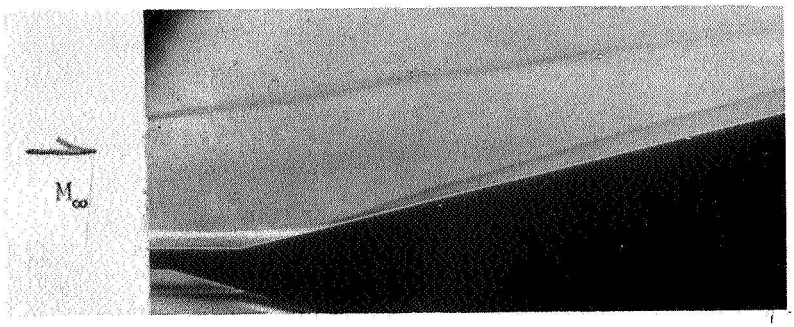

(a) Smooth leading-edge fin.

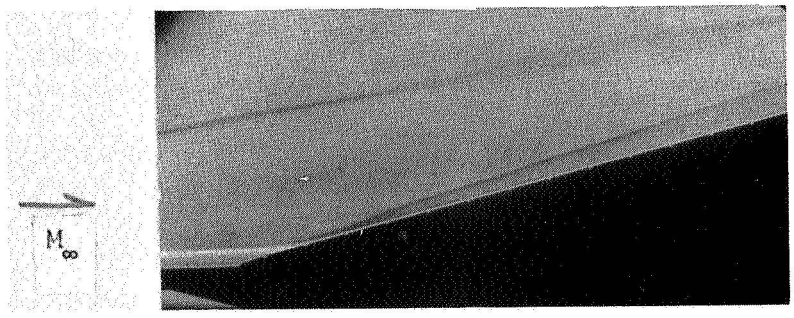

(b) Multislotted leading-edge fin. L-67-6630

Figure 4.- Schlieren photographs of flow in vicinity of intersection of fin and plate for both smooth and multislotted leading-edge fins. $M_\infty = 7.87$; $R_{\infty,D} = 1.12 \times 10^5$; $T_w/T_0 = 0.4$.

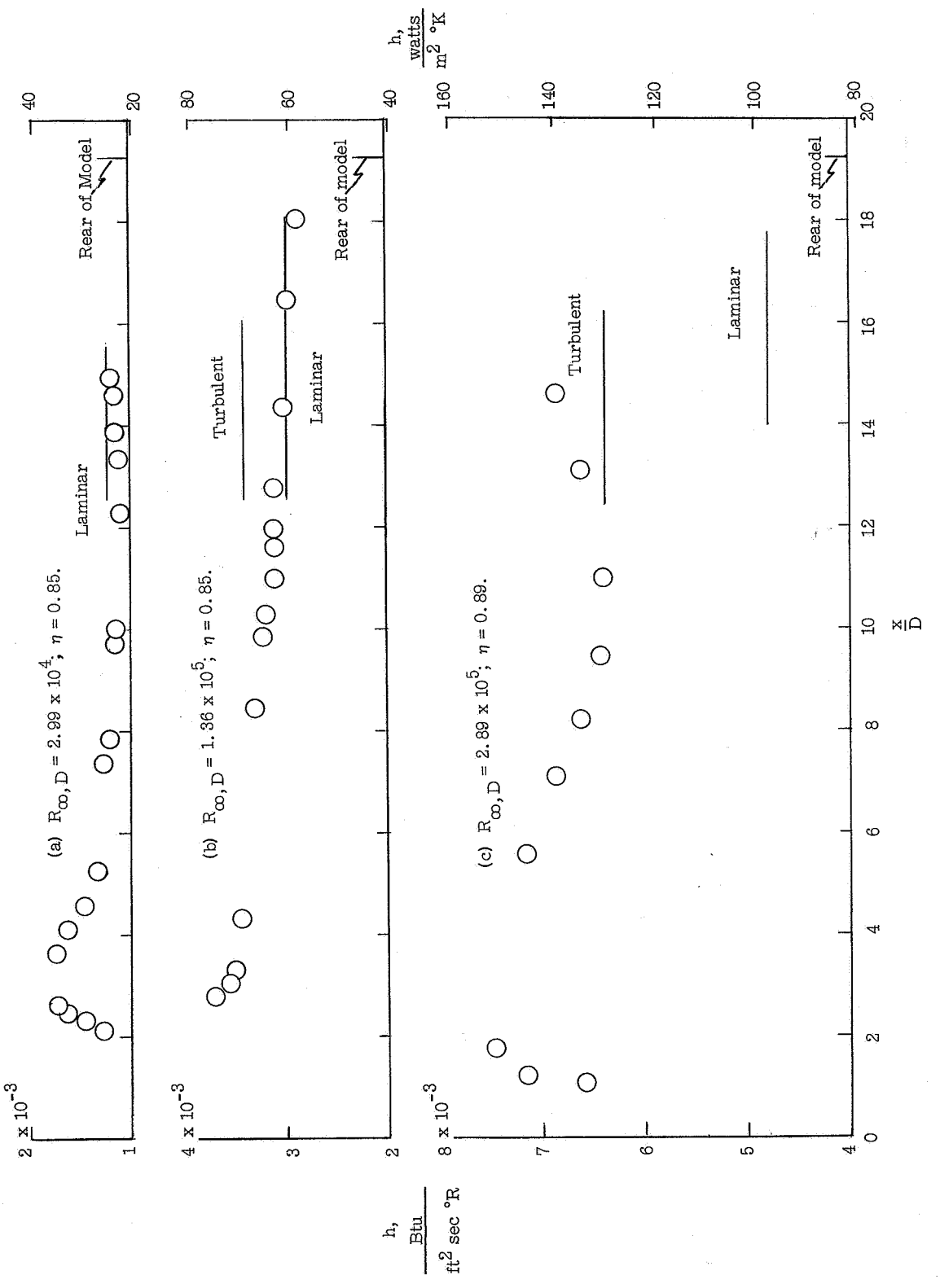

Figure 5.- Heat-transfer-coefficient distribution along fin stagnation line. Smooth leading edge. Theoretical levels shown are from swept cylinder theories of reference 2.

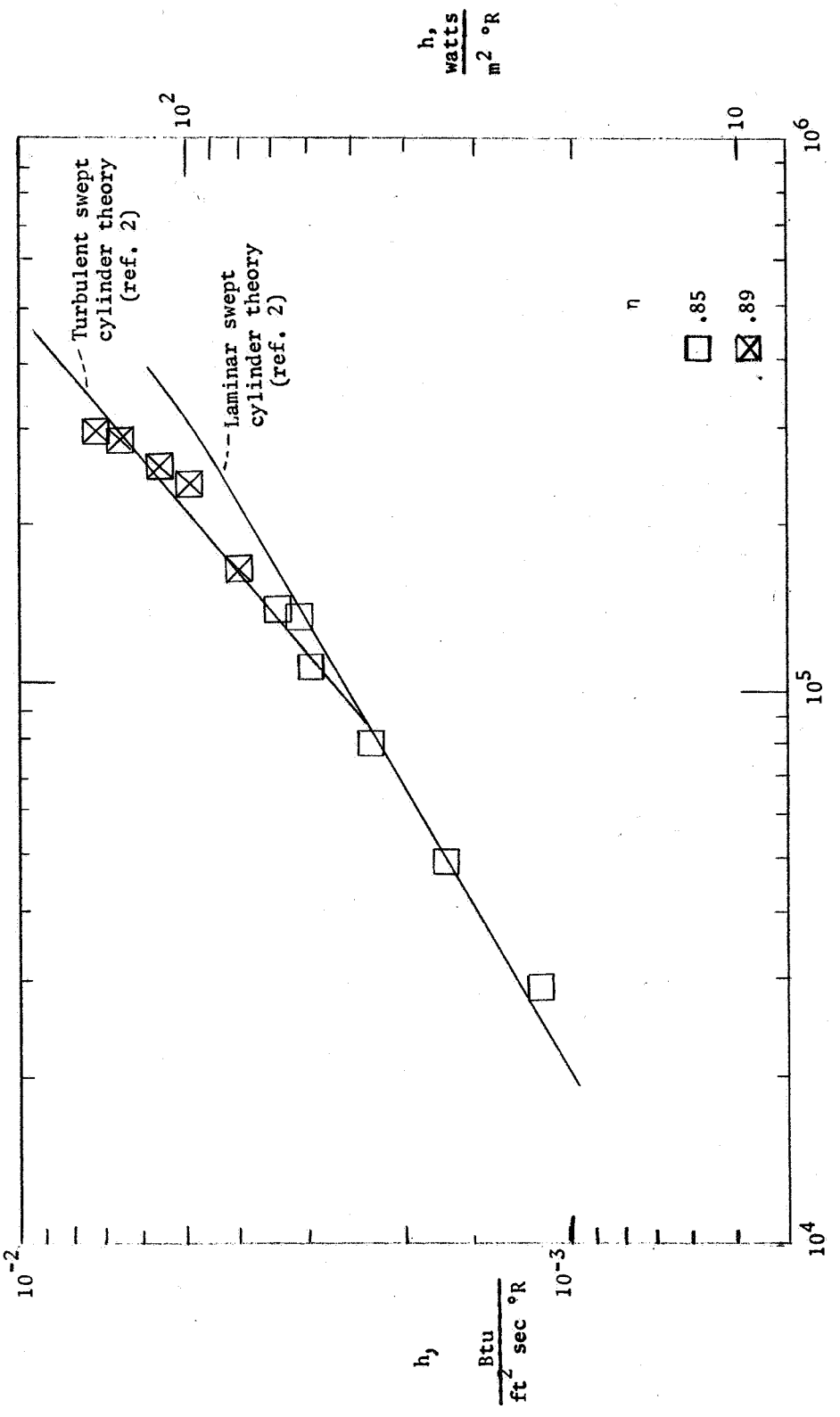

Figure 6.- Variation of stagnation-line heat-transfer coefficient with effective free-stream Reynolds number. $x/D \approx 12$; smooth model.

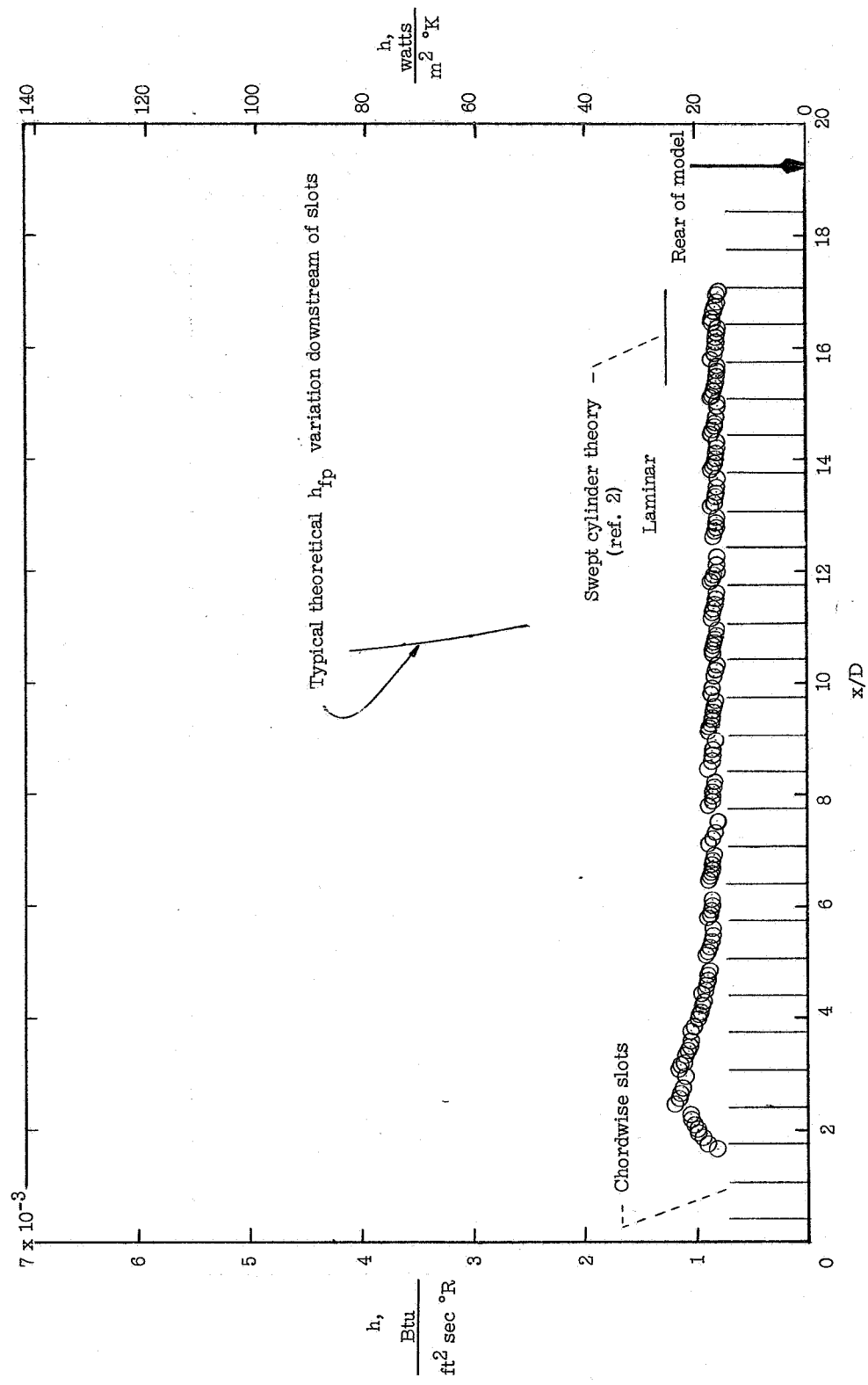

(a) $R_{\infty,D} = 2.99 \times 10^4$.

Figure 7.- Distribution of heat-transfer coefficient along stagnation line of multislotted fin. $\eta = 0.85$.

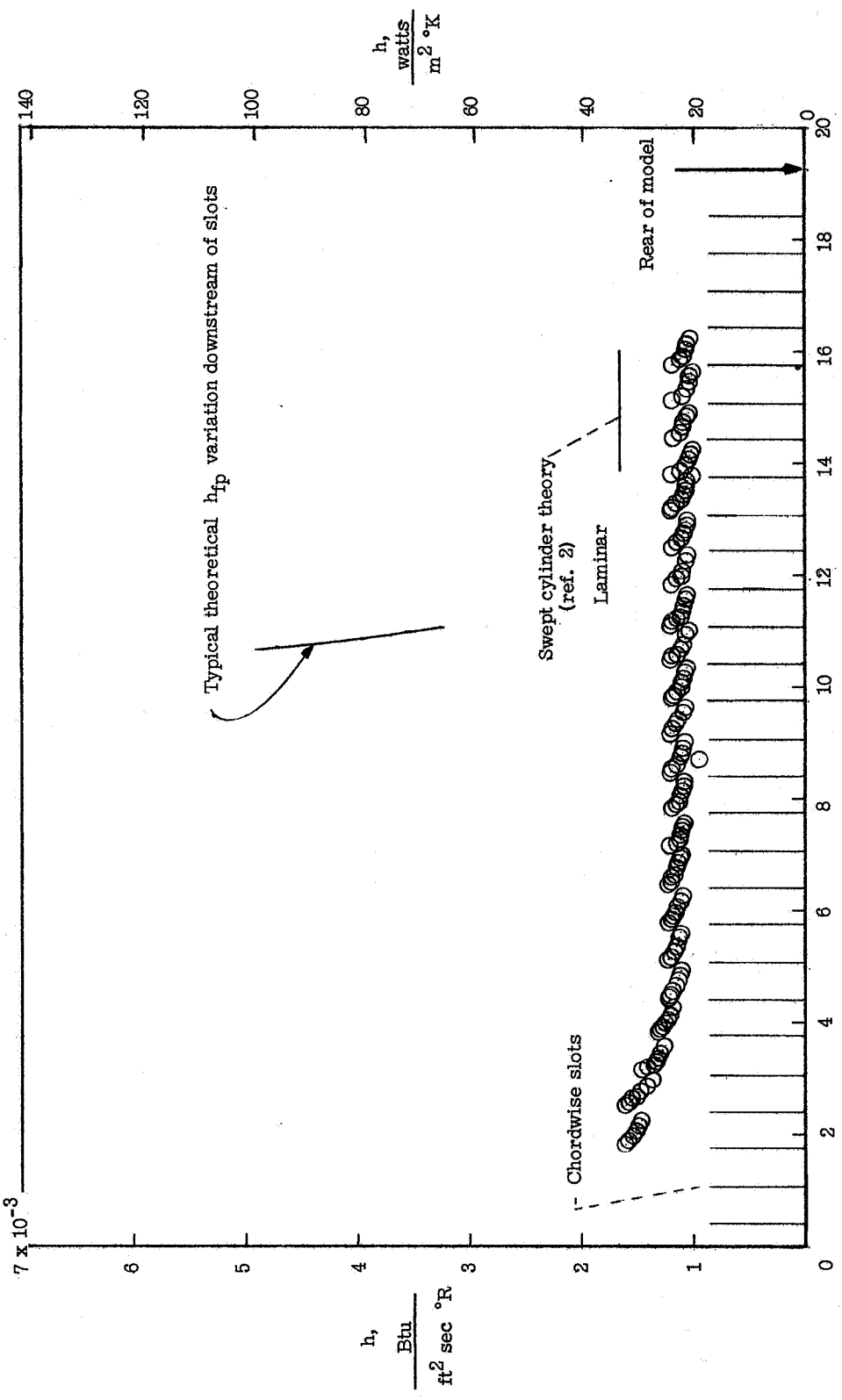

(b) $R_{\infty,D} = 4.95 \times 10^4$.

Figure 7.- Continued.

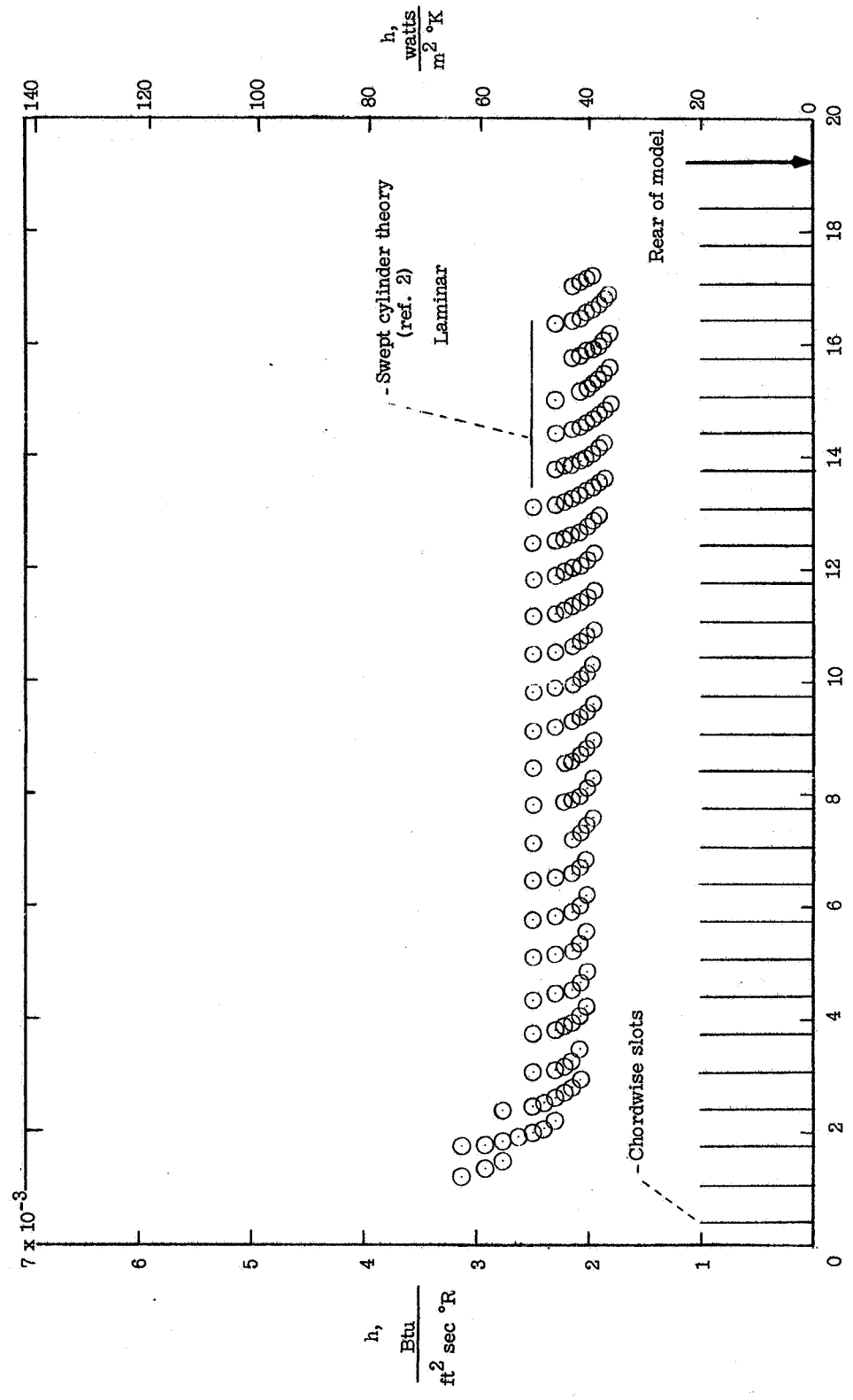

(c) $R_{\infty,D} = 1 \times 10^5$.

Figure 7.- Continued.

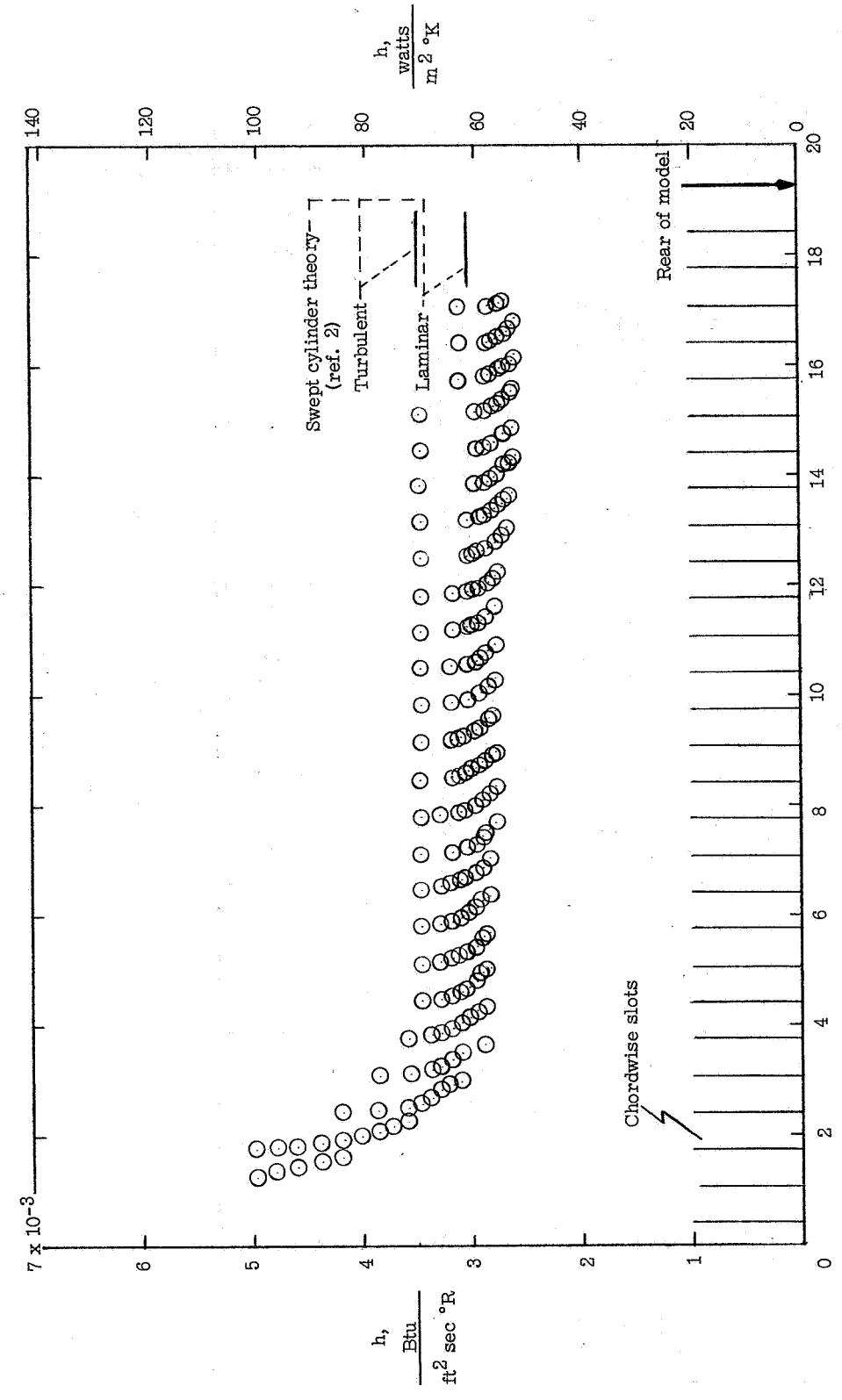

(d) $R_{\infty,D} = 1.41 \times 10^5$.

Figure 7.- Continued.

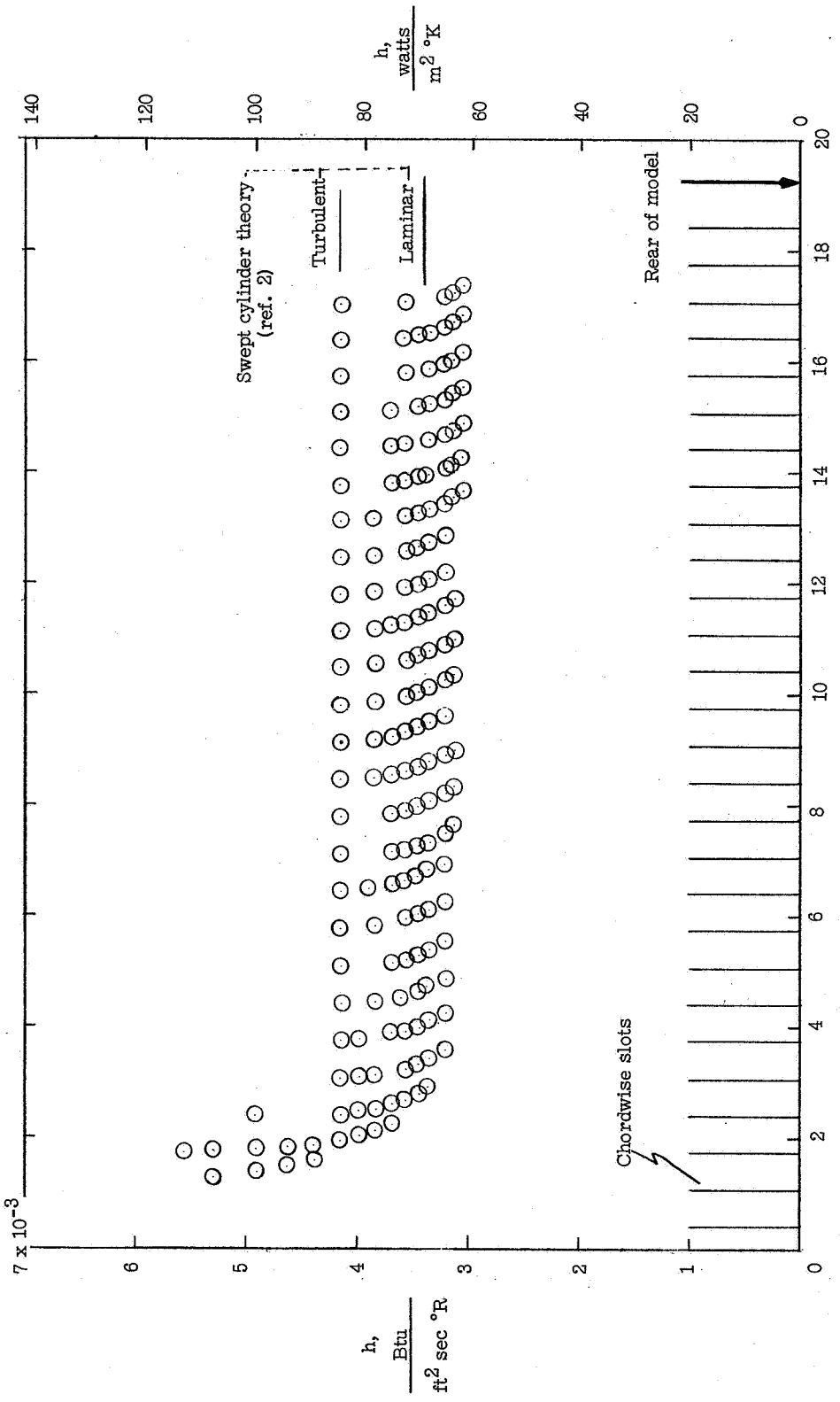

(e) $R_{\infty,D} = 1.74 \times 10^5$.

Figure 7.- Continued.

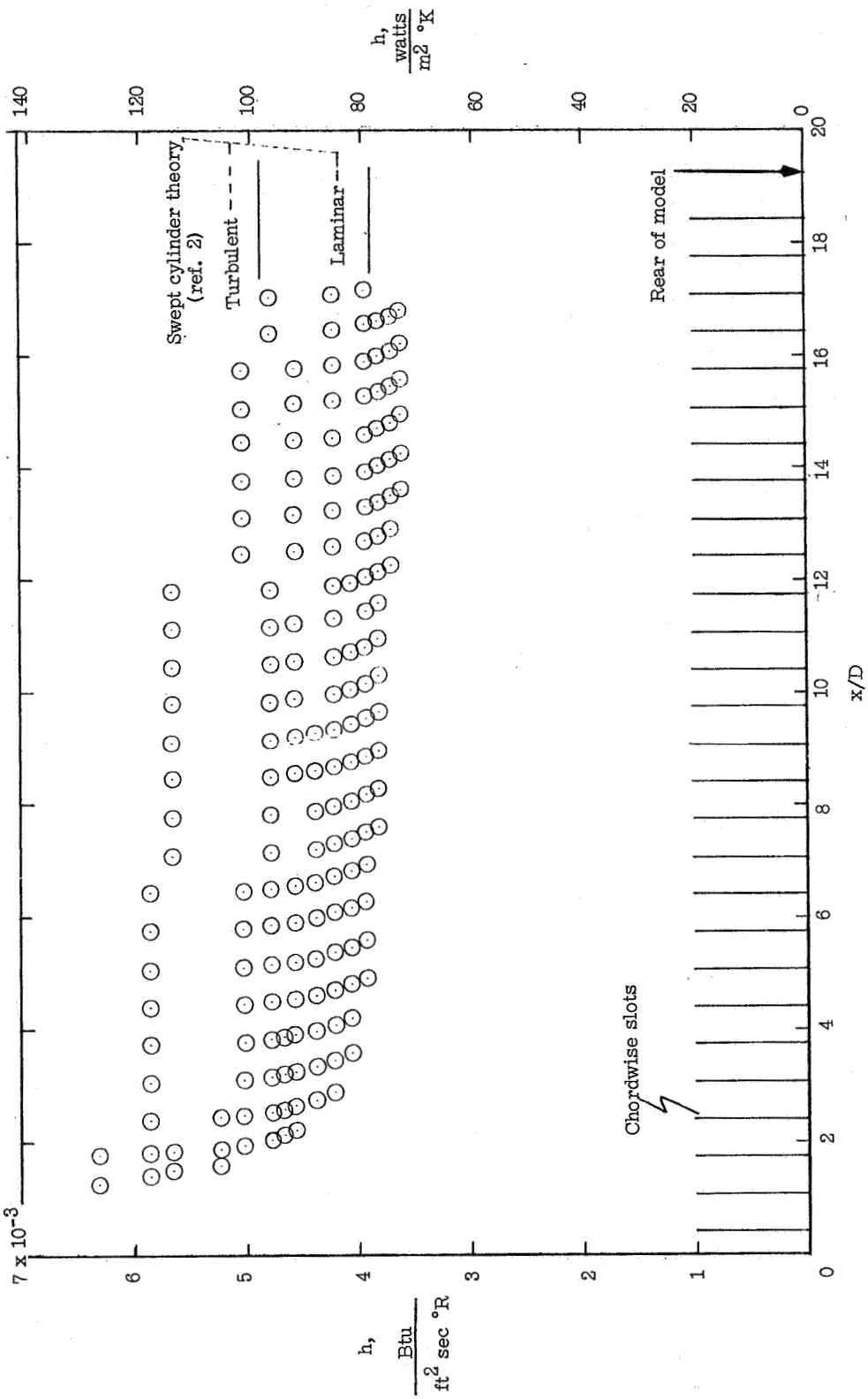

(f) $R_{\infty,D} = 2.1 \times 10^5$.

Figure 7.- Continued.

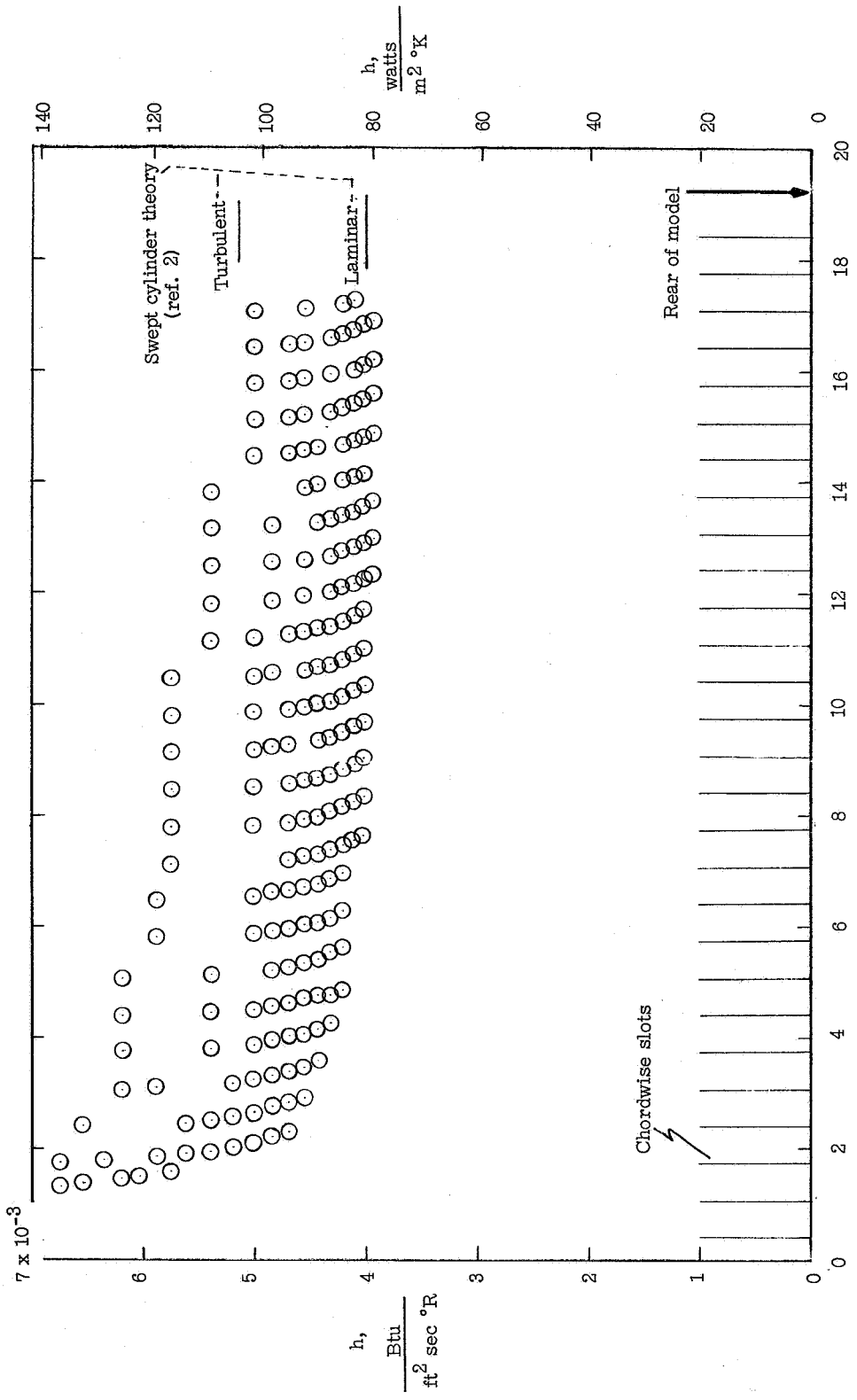

(g) $R_{\infty,D} = 2.23 \times 10^5$.

Figure 7.- Continued.

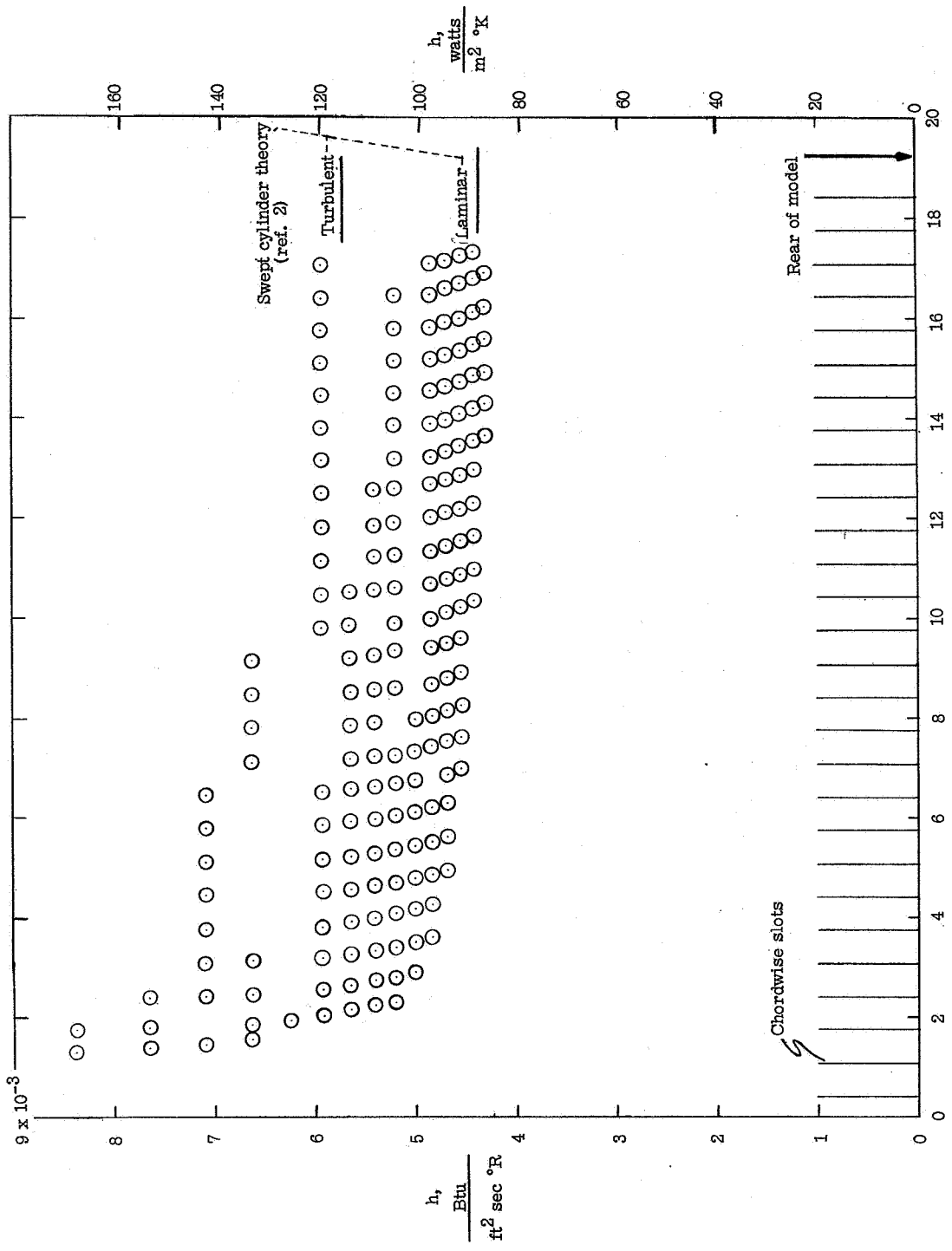

(h) $R_{\infty,D} = 2.52 \times 10^5$.

Figure 7.- Continued.

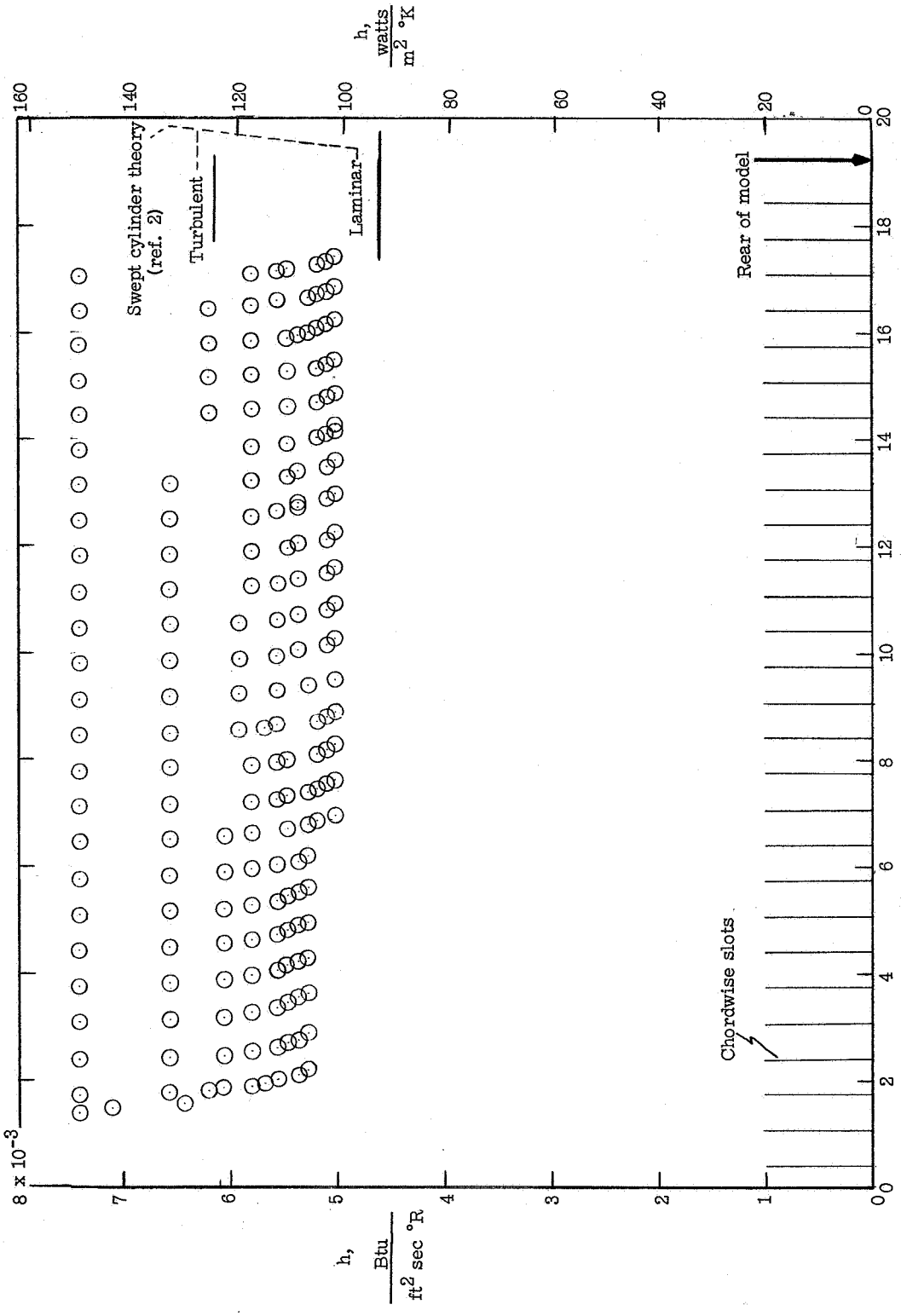

(i) $R_{\infty,D} = 2.75 \times 10^5$.

Figure 7.- Continued.

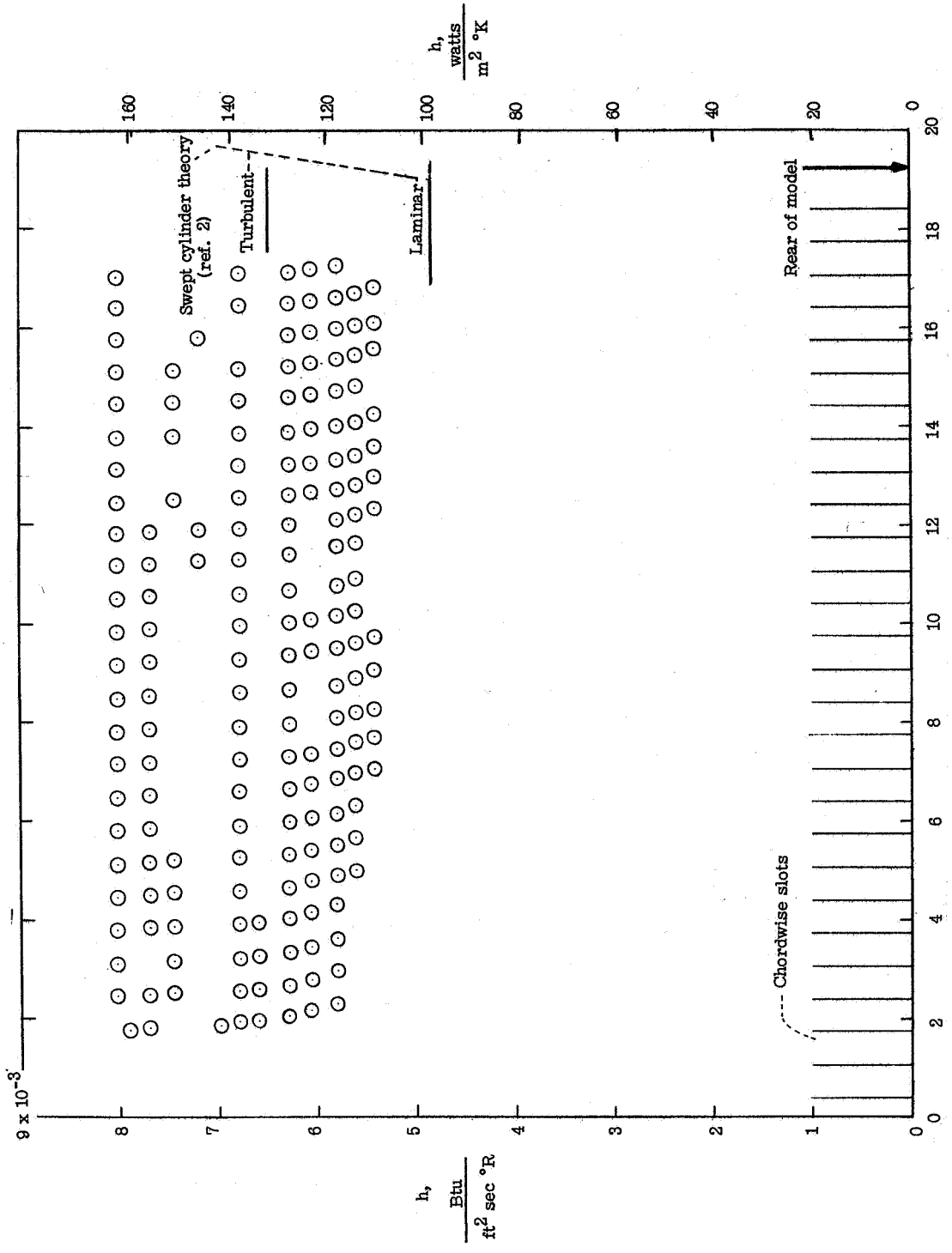

(j) $R_{\infty,D} = 2.96 \times 10^5$.

Figure 7.- Concluded.

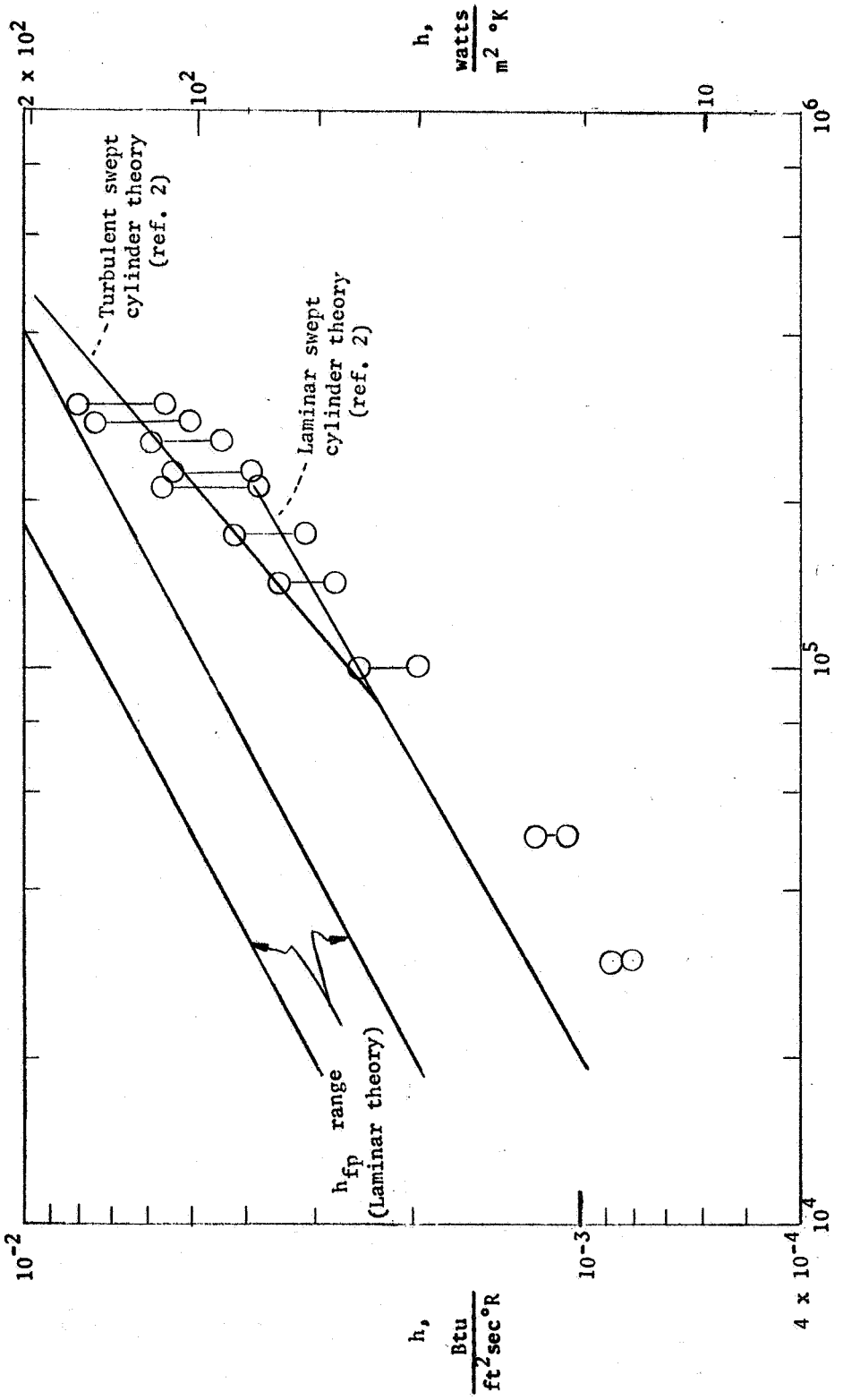

Figure 8.- Variation of maximum and minimum heat-transfer coefficient with Reynolds number for the multislotted leading-edge model. $x/D \approx 12$; $\eta = 0.85$.

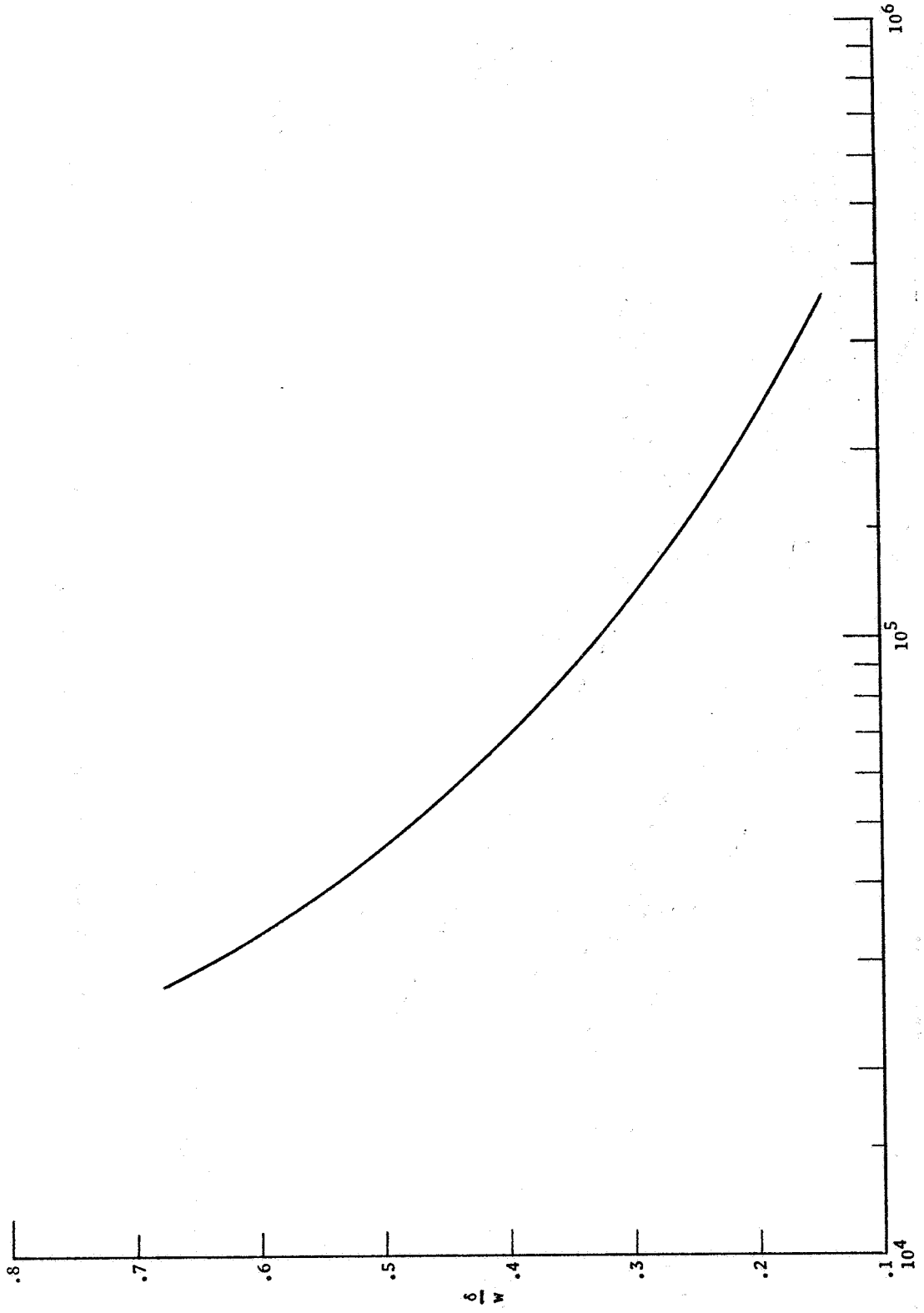

Figure 9.- Variation of ratio or laminar stagnation-line boundary-layer thickness to slot width with Reynolds number.

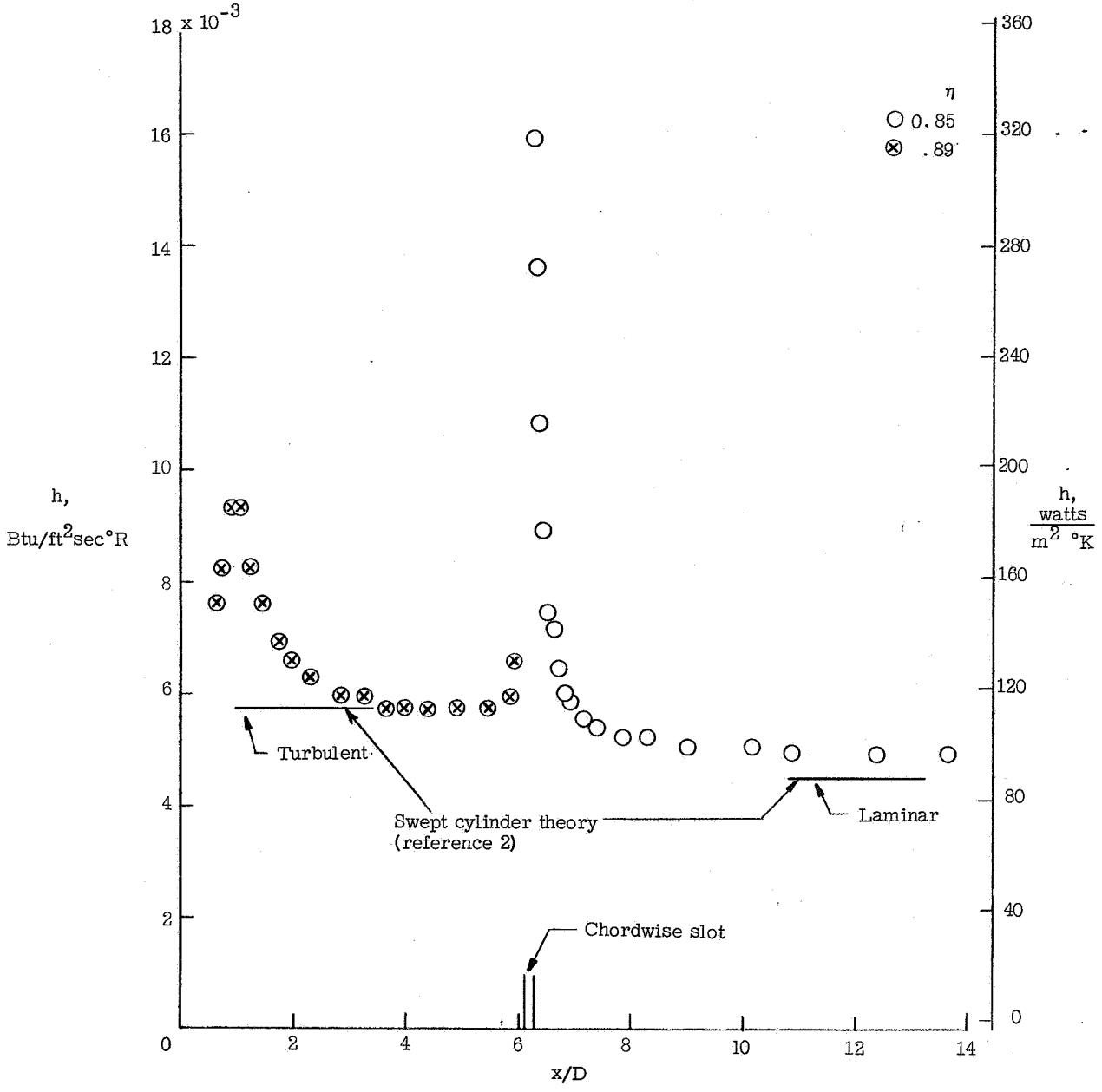

(a) $R_{\infty,D} = 2.62 \times 10^5$.

Figure 10.- Distribution of heat-transfer coefficient along stagnation line of single slotted fin.

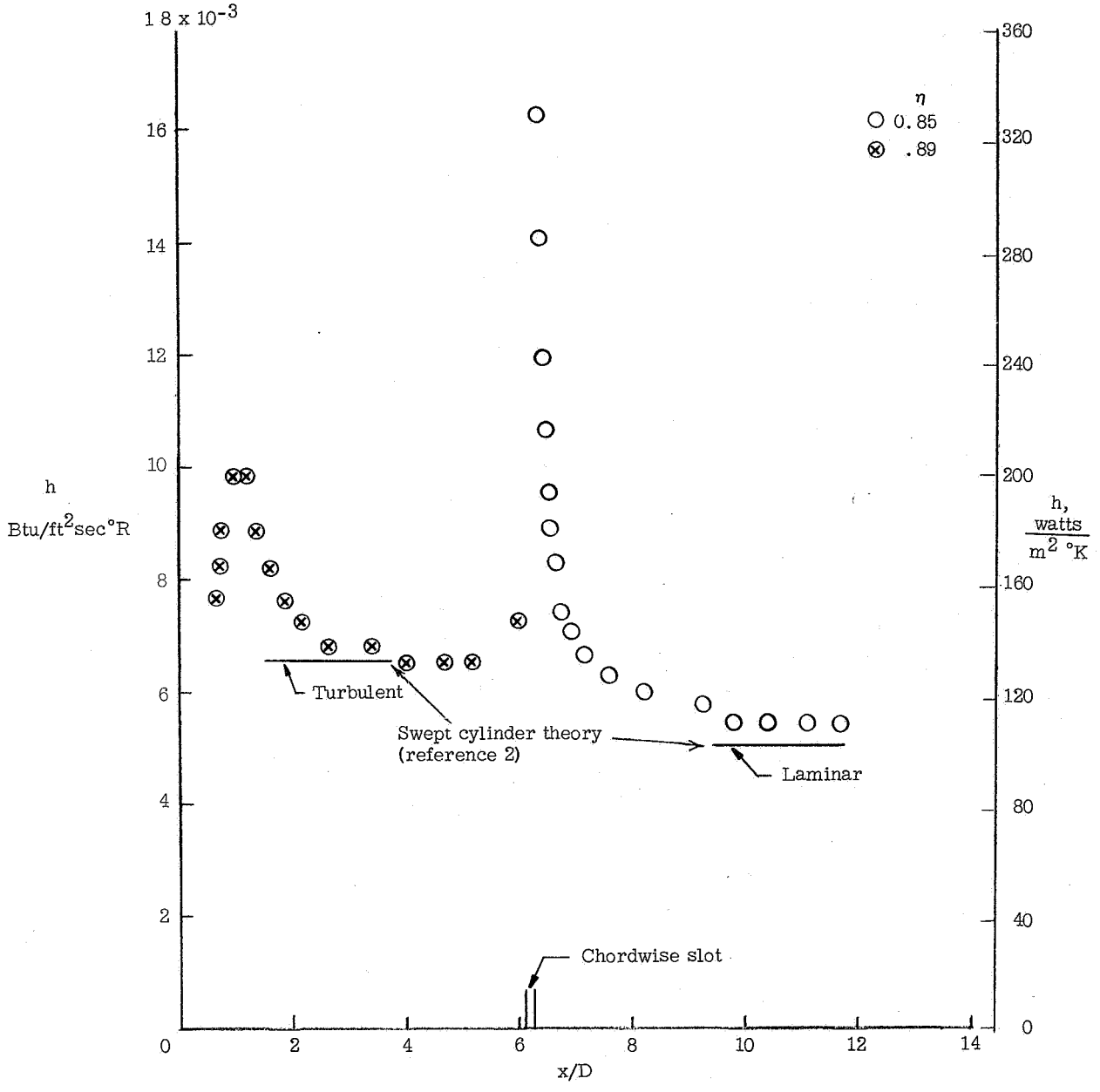

(b) $R_{\infty,D} = 2.96 \times 10^5$.

Figure 10.- Concluded.

Symbol	M_∞	T_w/T_o	D		Λ, deg	Configuration	Reference
			in.	cm			
○	6	0.46	1.06	2.69	70	Fin plate	16
□	7.4	.4	.75	1.905	78	Fin plate	Present data
◇	4.1	.75	.5	1.27	21, 39.7, 58.5, 49.5	Cylinder with end plate	17
△	4.1	.8	1.11	2.82	10, 20, 40, 60	Cylinder with end plate	2
↘	2.65 to 4.44	.8	2.8	7.1	45	Cylinder plate (cylinder swept back)	18
◺	3.5	.8	.75 to 3.5	1.905 to 8.88	12.87	Fin plate	19
⌓	7.95	.4	1.0	2.54	72	Small end plate cylinder	Present data (appendix)
◇	7.95 to 5.3	.4	1.0	2.54	45, 53, 60, 68	Cylinder plate	4
◇	6.0	.65	1.06	2.69	60	Fin plate	20
⌓	2 to 4.1	.85	.375	.952	38	Fin clyinder (flight)	21
○	6.0	.55	1.0	2.54	70	Fin plate	22
□	2.5 to 4.0	.65	.25, .5, .75	.635, 1.27, 1.905	45, 36.75	Fin cylinder (flight)	23
◇	8.0	.26	3.5	8.88	12.9	Fin plate	24
△	2.0	.65	.75	1.905	75	Fin cylinder (flight)	25
↙	3.9	1.1	1	2.54	30, 44	Cylinder	26
◹	4.4	.8	.1	.254	39, 75	Fin cylinder (flight)	27
◺	6.08	.5	1	2.54	65	Fin plate	28
◇	2.42	≈1.0	.394	1.0	18, 27, 36, 43, 50, 57, 64	Cylinder plate	29
◇	3.0	1.0	.078	.2	76	Fin plate	30

(a) Identification of symbols used on figures 11(b) and 11(c).

Figure 11.- Correlation of swept-leading-edge heat-transfer data from fin-plate or cylinder-plate configurations.

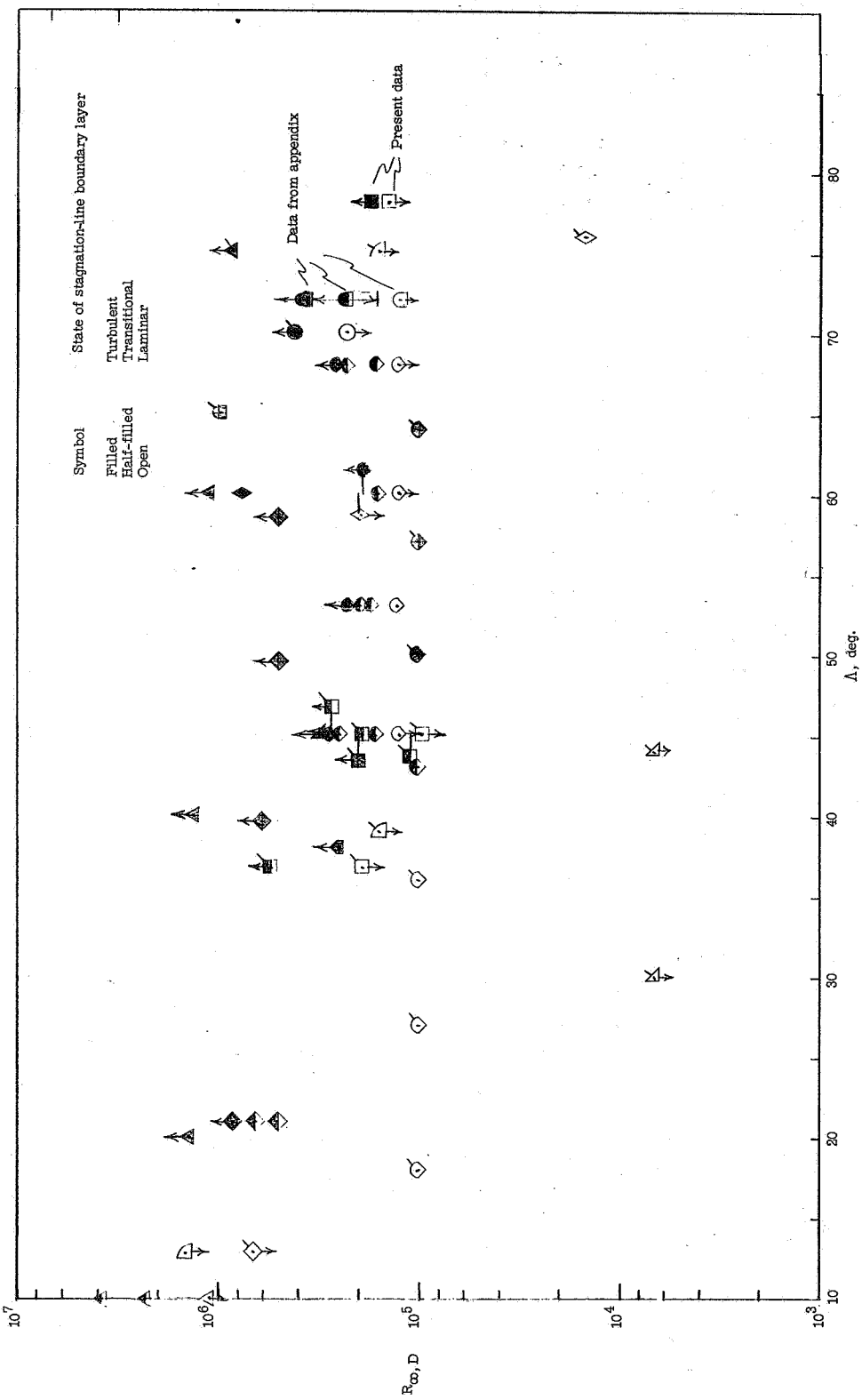

(b) Correlation in terms of simple $R_{\infty,D}$ parameter. Arrows indicate data at other $R_{\infty,D}$ values with same boundary-layer state.

Figure 11.- Continued.

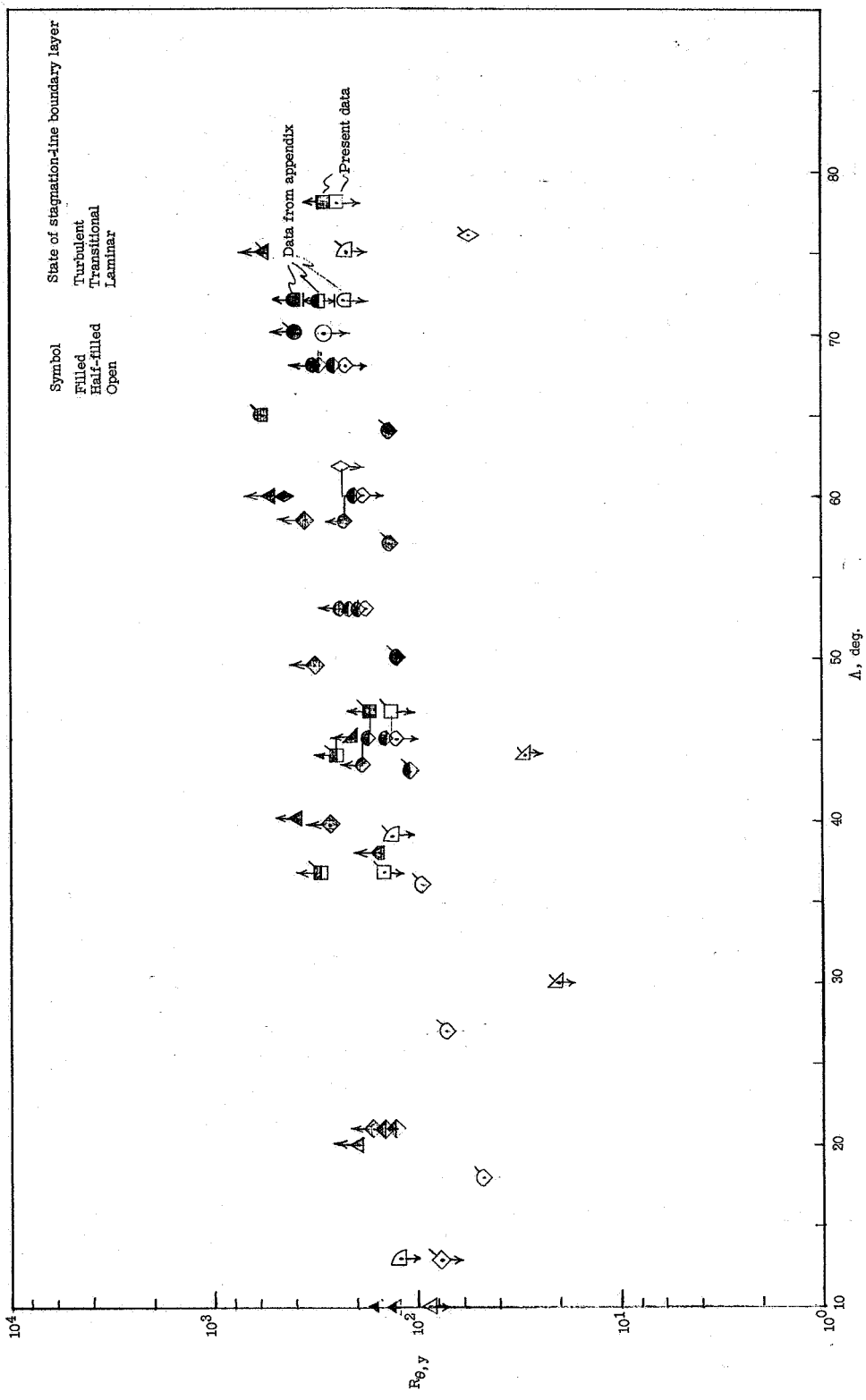

(c) Correlation in terms of $R_{\theta,y}$ parameter. Arrows indicate data at other $R_{\theta,y}$ values with same boundary-layer state.

Figure 11.- Concluded.

Symbol	M_∞	T_w/T_0	D		Λ, deg	Configuration	Reference
			in.	cm			
○	6.86	0.6	0.5	1.27	20, 40, 60, 75	Cylinder without end plate	31
□	2.65 to 4.44	.8	2.8	7.11	45	Cylinder without end plate (swept forward)	18
◇	8.0	.3	.754	1.91	73	Delta wing	7
△	9.6	.45	.75	1.9	70	Delta wing	32
◺	6.8	.8	.75	1.9	70	Delta wing	32
◺	4.95	.6	.5	1.27	60	Delta wing	33
◺	6.8, 9.6	.6	1	2.54	80	Delta wing	34
◇	8.08	.4	1.02	2.59	73	Delta wing	35
◇	3.51, 4.65	.8	1.0	2.54	70	Delta wing	36
◺	4.95	.6	.75	1.9	60	Delta wing	37
◺	9.86	.34	1.0	2.54	70	Delta wing	38
◇	9.6	.34	.1	.254	60, 75	Delta wing	39
◺	Up to 9.8	.1	.2	.508	82	Delta wing (flight)	40
◺	8.08	.34	1.5	3.81	60, 70, 80	Delta wing	41
◺	8.1	.4	1.6	4.06	73	Delta wing	42
◺	6.0	1.0	2.38	6.04	45, 55, 65	Fin with blunt prow	43
◺	8.0	.34	2.38	6.04	45, 55, 65	Fin with blunt prow	43
◇	4.0	1.0	2.38	6.04	45, 55, 65	Fin with blunt prow	43
◺	8	.34	2.38	6.04	30, 60	Fin with blunt prow	44
○	4	1.0	2.38	6.04	30, 50	Fin with blunt prow	44
□	6.08	.6	.626	1.59	75	Delta wing	45
◇	2.5, 3, 4	1.0	.04	.010	15, 30, 45, 60	Swept slab	1
△	10	.3	2	5.08	45	Swept slab	8

(a) Identification of symbols used in figures 12(b) and 12(c).

Figure 12.- Correlation of "undisturbed" swept-leading-edge heat-transfer data from research delta-wing models and cylinders without end plates.

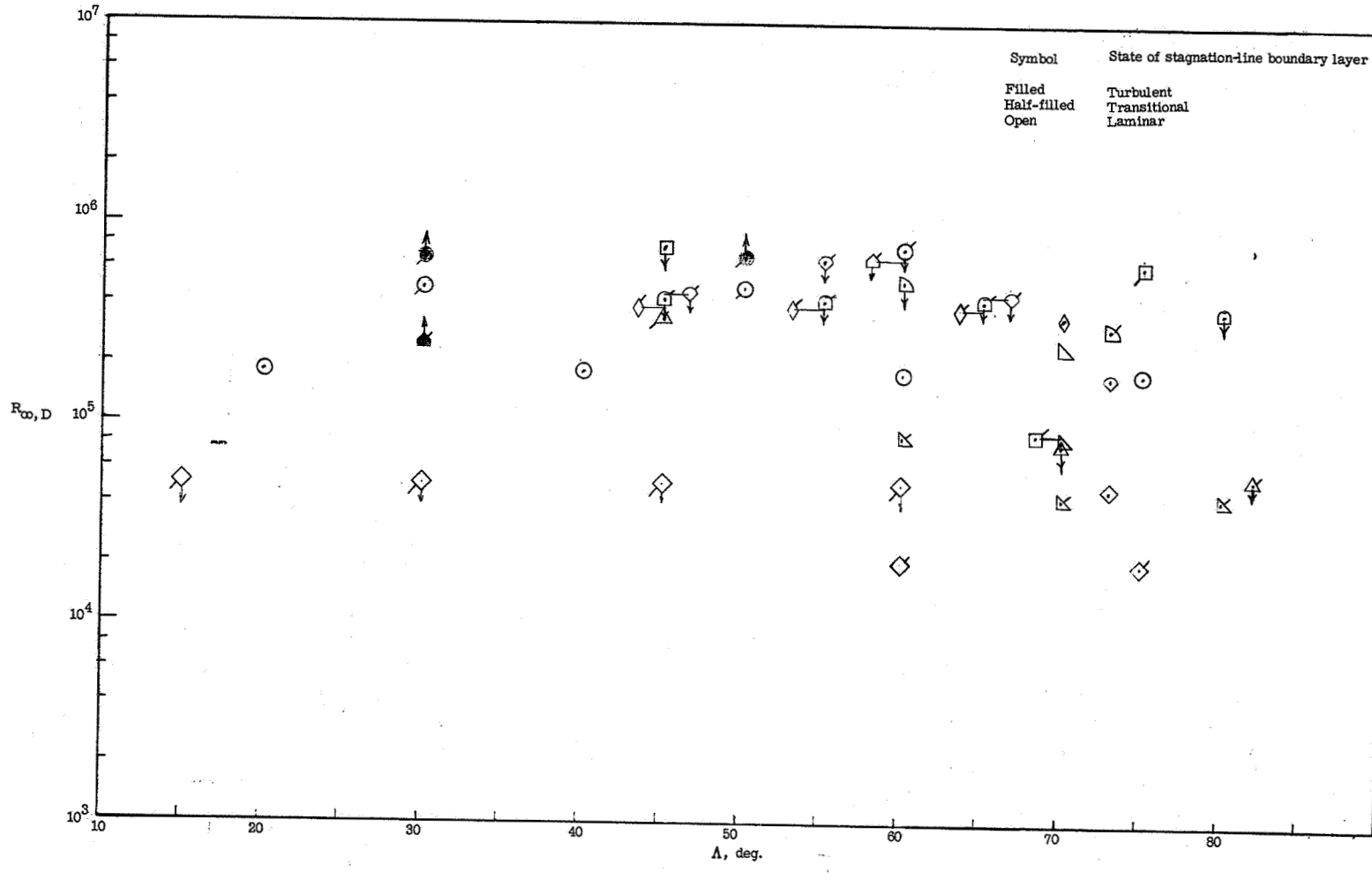

(b) Correlation in terms of simple $R_{\infty,D}$ parameter. Arrows indicate data at other $R_{\infty,D}$ values with same boundary-layer state.

Figure 12.- Continued.

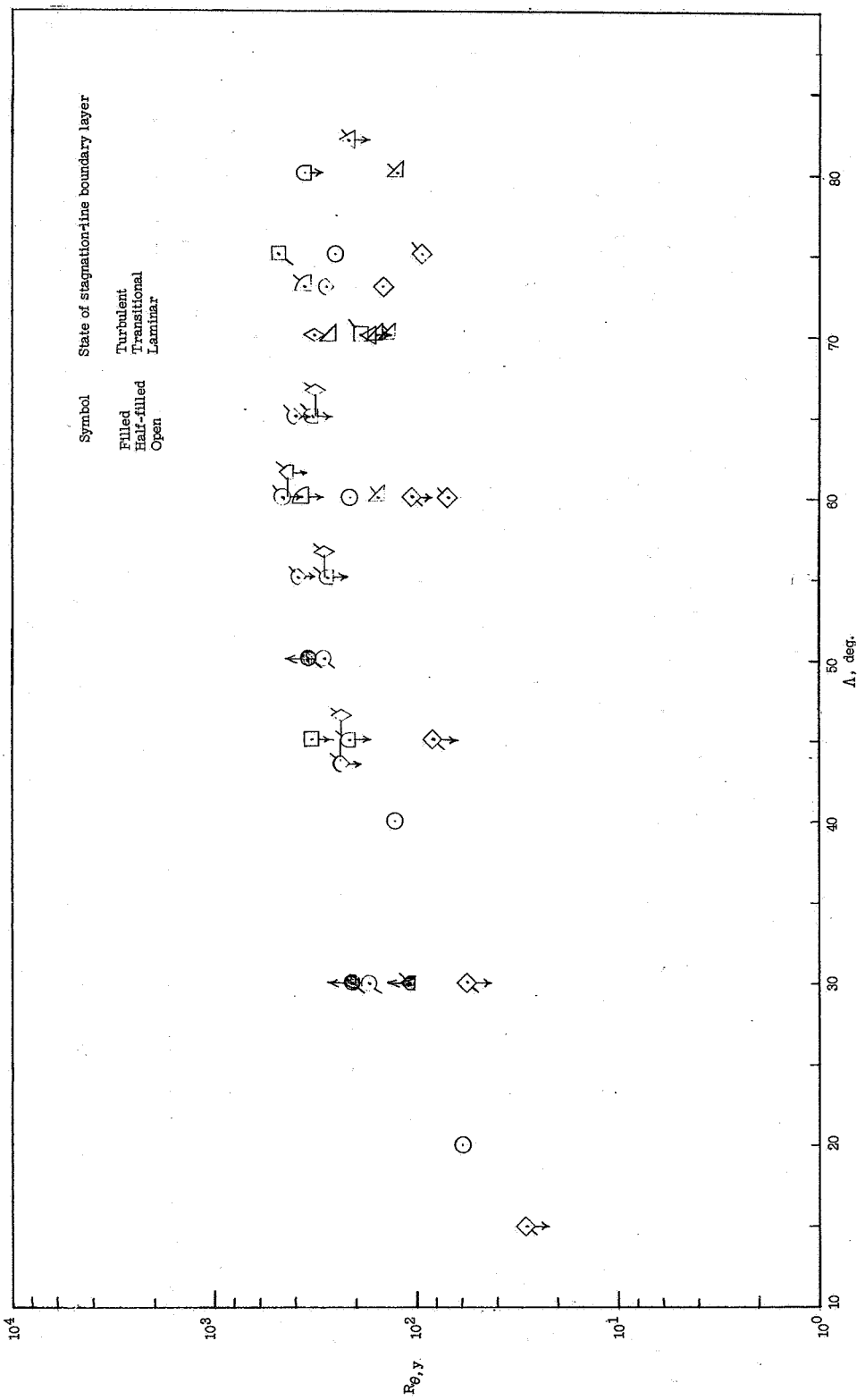

(c) Correlation in terms of $R_{\theta,y}$ parameter. Arrows indicate data at other $R_{\theta,y}$ values with same boundary-layer state.

Figure 12.- Concluded.

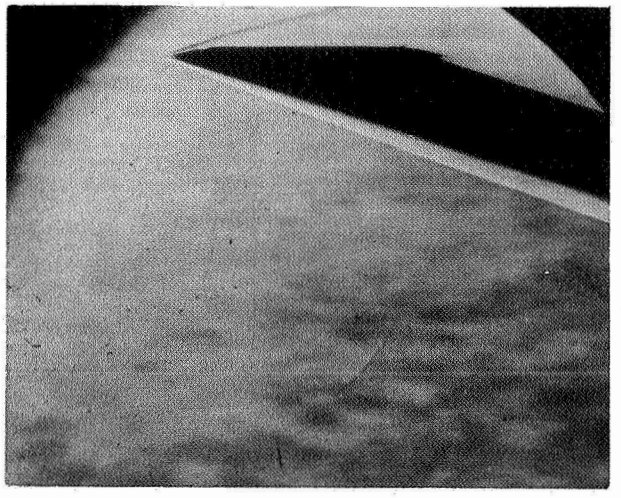

(a) $R_{\infty,D} = 3.36 \times 10^5$.

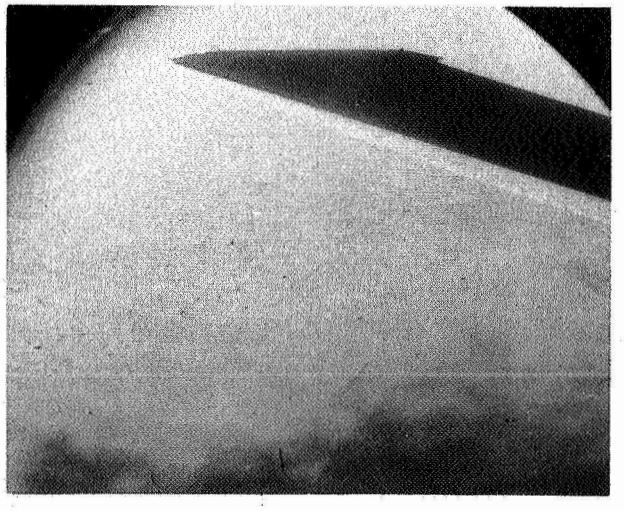

(b) $R_{\infty,D} = 8.2 \times 10^4$. L-67-6631

Figure 13.- Schlieren photographs of flow over 72° swept cylinder. $M_\infty = 7.95$.

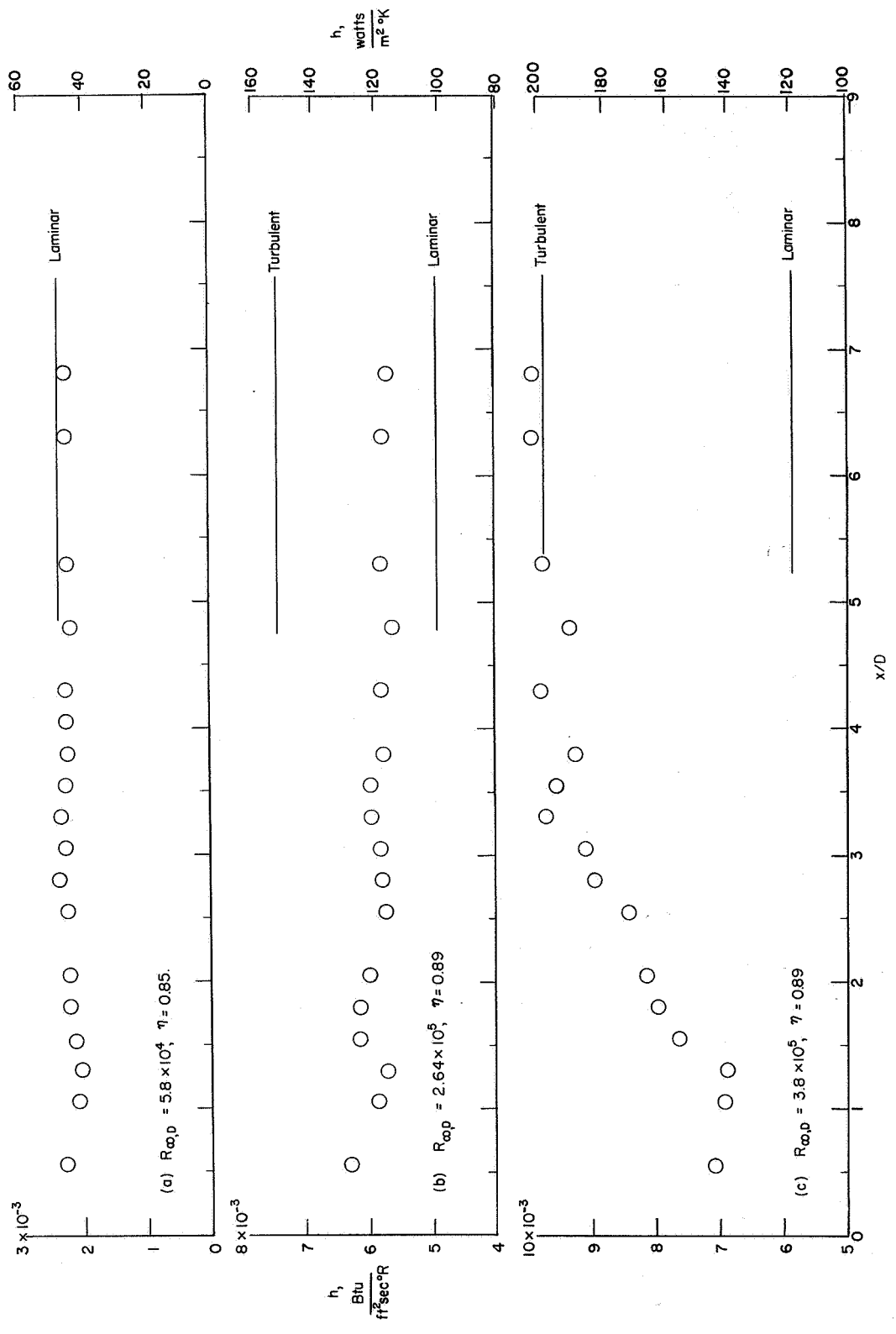

Figure 14.- Stagnation-line heat-transfer distribution for swept right circular cylinder. $\Lambda = 72^0$, $M_\infty = 7.95$, small end plate attached to tip and alined with free stream. Theoretical levels shown are from swept cylinder theories of reference 2.

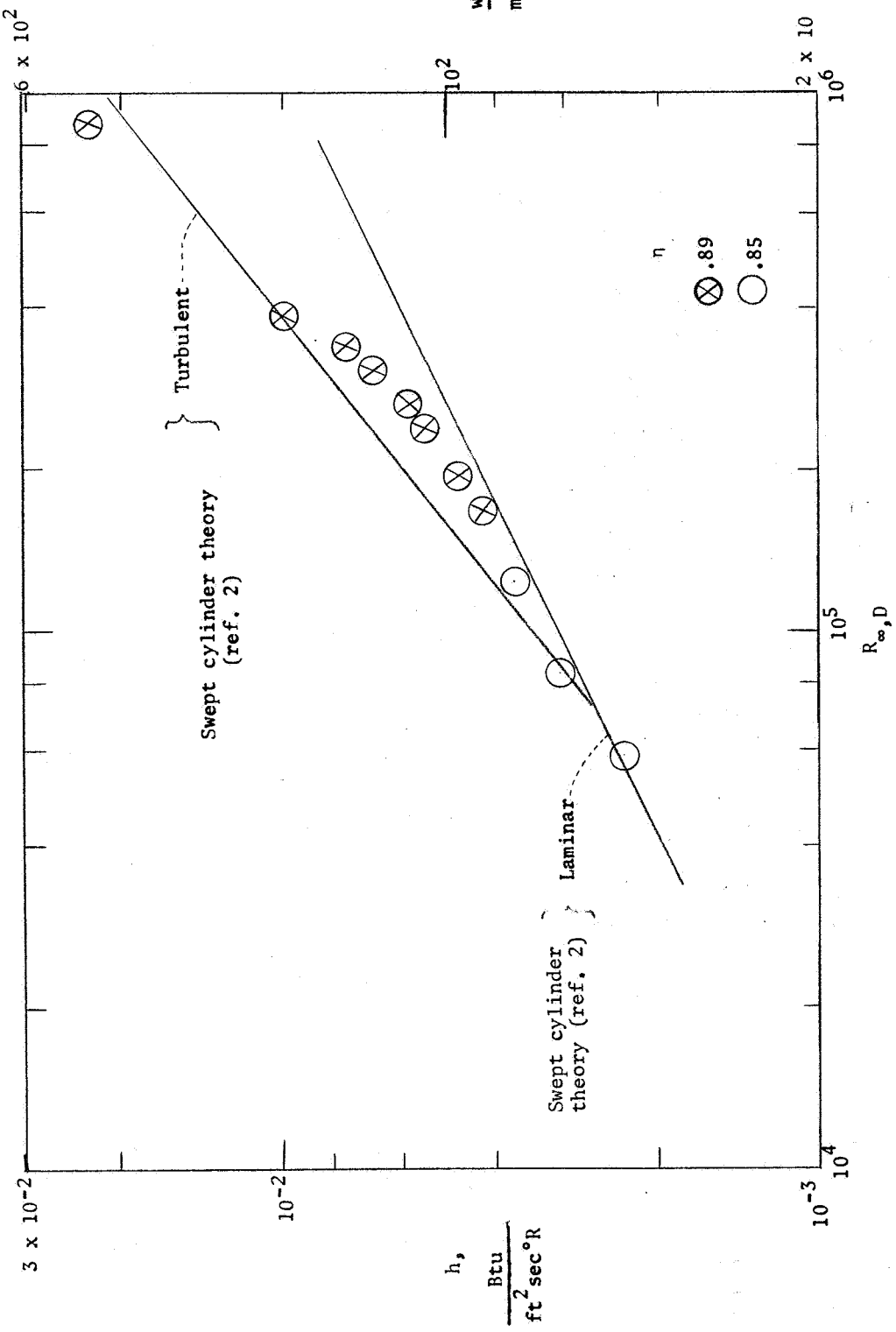

Figure 15.- Stagnation-line heat-transfer coefficient as a function of free-stream Reynolds number. $x/D = 4.3$; $M_\infty = 7.95$; $\Lambda = 72^0$; small end plate.

"The aeronautical and space activities of the United States shall be conducted so as to contribute . . . to the expansion of human knowledge of phenomena in the atmosphere and space. The Administration shall provide for the widest practicable and appropriate dissemination of information concerning its activities and the results thereof."

—National Aeronautics and Space Act of 1958

NASA SCIENTIFIC AND TECHNICAL PUBLICATIONS

TECHNICAL REPORTS: Scientific and technical information considered important, complete, and a lasting contribution to existing knowledge.

TECHNICAL NOTES: Information less broad in scope but nevertheless of importance as a contribution to existing knowledge.

TECHNICAL MEMORANDUMS: Information receiving limited distribution because of preliminary data, security classification, or other reasons.

CONTRACTOR REPORTS: Scientific and technical information generated under a NASA contract or grant and considered an important contribution to existing knowledge.

TECHNICAL TRANSLATIONS: Information published in a foreign language considered to merit NASA distribution in English.

SPECIAL PUBLICATIONS: Information derived from or of value to NASA activities. Publications include conference proceedings, monographs, data compilations, handbooks, sourcebooks, and special bibliographies.

TECHNOLOGY UTILIZATION PUBLICATIONS: Information on technology used by NASA that may be of particular interest in commercial and other non-aerospace applications. Publications include Tech Briefs, Technology Utilization Reports and Notes, and Technology Surveys.

Details on the availability of these publications may be obtained from:

SCIENTIFIC AND TECHNICAL INFORMATION DIVISION

NATIONAL AERONAUTICS AND SPACE ADMINISTRATION

Washington, D.C. 20546